Nanoparticle radio-enhancement: principles, progress and application to cancer treatment

Zdenka Kuncic, Sandrine Lacombe

TOPICAL REVIEW • OPEN ACCESS

Nanoparticle radio-enhancement: principles, progress and application to cancer treatment

IOP Publishing Phys. Med. Biol. 63 (2018) 02TR01 (27pp) https://doi.org/10.1088/1361-6560/aa99ce

Physics in Medicine & Biology

IPEM Institute of Physics and Engineering in Medicine

OPEN ACCESS

TOPICAL REVIEW

Nanoparticle radio-enhancement: principles, progress and application to cancer treatment

Zdenka Kuncic[1] and Sandrine Lacombe[2]

[1] School of Physics and Sydney Nano Institute, University of Sydney, Sydney, NSW 2006, Australia
[2] Institut des Sciences Moléculaires d'Orsay (UMR 8214) University Paris-Sud, CNRS, University Paris-Saclay, 91405 Orsay cedex, France

E-mail: zdenka.kuncic@sydney.edu.au

Keywords: nanoparticles, radio-enhancement, radiation physics, radiotherapy, proton therapy, particle therapy, theranostics

RECEIVED
4 June 2017

REVISED
12 October 2017

ACCEPTED FOR PUBLICATION
10 November 2017

PUBLISHED
9 January 2018

Abstract

Enhancement of radiation effects by high-atomic number nanoparticles (NPs) has been increasingly studied for its potential to improve radiotherapeutic efficacy. The underlying principle of NP radio-enhancement is the potential to release copious electrons into a nanoscale volume, thereby amplifying radiation-induced biological damage. While the vast majority of studies to date have focused on gold nanoparticles with photon radiation, an increasing number of experimental, theoretical and simulation studies have explored opportunities offered by other NPs (e.g. gadolinium, platinum, iron oxide, hafnium) and other therapeutic radiation sources such as ion beams. It is thus of interest to the research community to consolidate findings from the different studies and summarise progress to date, as well as to identify strategies that offer promising opportunities for clinical translation. This is the purpose of this Topical Review.

List of abbreviations and acronyms

AuNP	Gold nanoparticle
BP	Bragg peak
GdNP	gadolinium based nanoparticle
HfNP	Hafnium based nanoparticle
MRI	Magnetic resonance imaging
LET	Linear energy transfer
NP	Nanoparticle
NRE	Nano-radio-enhancer
PtNP	Platinum nanoparticle
SOBP	Spread-out Bragg peak
SPION	Super-paramagnetic iron-oxide nanoparticle

1. Introduction

Nanoparticle strategies for enhancing the therapeutic efficacy of cancer treatment modalities continue to be actively investigated (Davis *et al* 2008, Mura and Couvreur 2012). In the context of radiotherapy treatment, high atomic number (Z) nanoparticles (NPs) have attracted increasing interest for their capacity to enhance radiation damage. Indeed, the introduction of high-Z NPs into a tumour offers the possibility of amplifying radiation damage effects selectively in the tumour as compared to healthy tissues, thus enhancing therapeutic efficacy. The property specific to high-Z nanoparticles is the enhancement of electron release in the medium compared to water due to atomic excitation by incident radiation. Note that high-Z NPs have been referred to as radiosensitisers, similar to drugs that sensitise cells to radiation (e.g. DNA repair drugs). In this review, we distinguish these two categories of agents and refer to NPs used to amplify radiation effects as 'nano-radio-enhancers' (NREs).

Most studies to date have focused on gold NPs of different sizes, shapes and surface coatings, which offer the advantage of being easily synthesised and stable, as well as exhibiting good biocompatibility and

pharmacokinetics (Jiang *et al* 2008, Toy *et al* 2014), as well as the capacity to internalise within cells and enhance radiation effects therein (e.g. Chithrani *et al* (2010) and Bhattarai *et al* (2017)). Other NPs have been developed in parallel including theranostic agents, which are now attracting growing interest for their potential to enhance not only targeted radiation effects but also contrast in magnetic resonance imaging and other imaging modalities (e.g. Luchette *et al* (2014)).

1.1. Motivation and rationale for this review

This Topical Review is motivated by the rapidly increasing number of studies investigating the potential of NREs to enhance external beam radiotherapy (photons and ions) in a clinical setting. While a number of reviews of this topic have been published in the literature, these have focused almost exclusively on gold NPs and photon irradiation (e.g. Hainfeld *et al* (2008), Butterworth *et al* (2012, 2013), Jain *et al* (2012) and Schuemann *et al* (2016)). With recent developments using other NREs, particularly gadolinium, which is a theranostic agent (reviewed by Sancey *et al* (2014) and Lux *et al* (2015)), and using other radiation treatment modalities such as proton therapy and heavy ion therapy, there is a need to:

i. consolidate our understanding of and rationalise the various approaches to nano-enhanced photon and particle based radiation therapies;
ii. identify strategies to support the next phase of development of nano-enhanced radiation therapy approaches with high potential for clinical translation;
iii. support the development of relatively under-explored capabilities for nanoparticle radio-enhancement combined with particle therapy;
iv. expose the added value of emerging opportunities such as internal radionuclide targeted therapy techniques combined with nano-agents and new nano-carriers as highly promising tumour targeting theranostic and patient adaptable platforms.

1.2. Scope of review

This review aims to provide:

– an up-to-date overview of the current understanding of the principles of high-Z nanoparticle activation by low-energy (keV) and high-energy (MeV) photons, as well as by electrons and incident ions, and the subsequent impact on the surrounding biological medium, with a focus on the initial physical processes involved;
– a summary of progress to date from experimental, simulation and modeling studies investigating radio-enhancement effects by gold NPs activated by photons or ions;
– a review of the development of other emerging and promising NREs, such as gadolinium based nano-agents, platinum nanoparticles, as well as hafnium oxide, iron oxide, cerium oxide and nanodiamonds;
– an overview of recent simulation, theoretical and modeling studies on radio-enhancement by NREs in general.

The structure of this review is as follows: section 2 presents the physical principles underlying high-Z nanoparticle radio-enhancement; sections 3–5 review the progress made to date from multiscale experimental studies—from *in vivo* to molecular and cellular scales—that have contributed to the increasing interest in NREs to improve photon and also particle beam radiation therapy; section 6 summarises corresponding modeling studies for incident photons and ions; and section 7 briefly summarises emerging strategies that present particularly promising opportunities for clinical translation. Finally, in section 8, we draw the main conclusions from our review and present our own perspective on the outlook for nanoparticle-enhanced radiation therapies.

2. Physical processes

The physical processes involved in the interactions of photons and ions with condensed matter have been extensively presented in the literature (see e.g. Hatano *et al* (2010)).

Briefly, the physical stage consists of the interaction of the primary beam (typically photons or fast ions) as well as the interaction of secondary particles (photons and electrons) produced along the primary radiation trajectory with the high-Z constituent atoms of nanoparticles embedded in biological tissue. This early excitation/ionisation stage is promptly followed by the de-excitation of the system via redistribution/rearrangement of electronic states, resulting in fluorescent photon emission (predominantly K-shell transitions) and Auger electron emission (predominant for inner shells other than the K orbital) (Evans 1955). Provided they are emitted in a dense medium (nanoparticle or biosystem), these secondary photons and electrons of energies ranging from

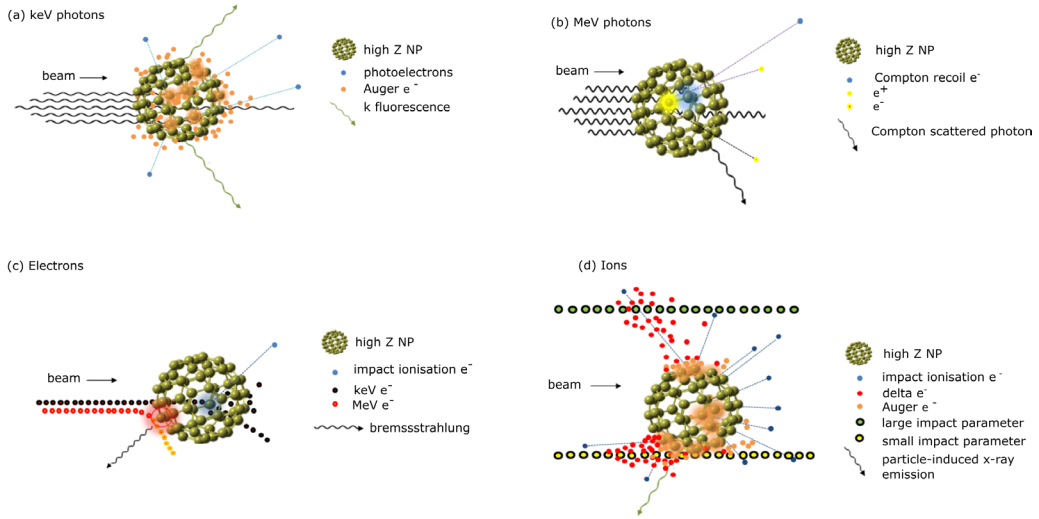

Figure 1. Schematic illustration of inelastic interactions with a high-Z nanoparticle for: (a) incident keV photons (orange clouds represent photoelectric events); (b) incident MeV photons (blue and yellow clouds represent Compton scatter and pair production events, respectively); (c) incident electrons (blue and red clouds represent large and small impact parameters leading to ionisation and bremsstrahlung, respectively); and (d) inicident ions (orange clouds indicate impact ionisation events). Image provided by Gholami, University of Sydney. Reproduced with permission from Y Gholami.

few eV (Auger electrons) to MeV (delta electrons) may successively ionise surrounding biomolecules as well as neighbouring nanoparticles. This cascade is expected to result in the enhancement of the radiation-induced perturbation highly localised to the nanoparticle-loaded biosystem. The basics of these processes are represented schematically in figure 1 and summarised in this section.

2.1. Interaction of photons with high-Z nanoparticles

Photoelectric absorption is the dominant interaction process of incident keV energy photons (typically up to ≈500 keV) with high-Z atoms ($Z \approx 60$–80 amu). The most studied high-Z nanoparticles considered as NREs are typically comprised of gold ($Z = 79$), platinum ($Z = 78$), hafnium ($Z = 72$), or gadolinium ($Z = 64$). The photoelectric cross-section strongly depends on Z, especially at photon energies E just above the absorption edges of the atom, where $\sigma \propto (Z/E)^n$, with $n \cong 3$–4. Thus, high-Z nanoparticles are able to transfer energy from radiation to the medium, through photoabsorption and subsequent electronic emission, much more effectively than water.

Ejection of a photoelectron, in principle from any shell, results in an electronic perturbation around the nanoparticle. Multiple photoelectrons emitted from many atoms in a high-Z NP (and indeed from multiple NPs) can thus give rise to an enhancement in dose, relative to that which would be measured without the presence of NPs. However, an additional enhancement effect arises from the ensuing atomic de-excitation processes (discussed below in section 2.3) that amplify the electronic perturbations in the immediate vicinity of NPs. We refer to this as 'nanoscale enhancement' of the radiation effects. The range of the ejected photoelectron is determined by the difference between E and the shell binding energy, E_B. For example, a 100 keV photon incident on a gold atom ($Z = 79$) is most likely to eject an electron from the K-shell ($E_K \approx 80.75$ keV). As a result, a photoelectron, which is ejected with a kinetic energy of 19.25 keV, may travel to a range in water of approximately 9 μm, which is comparable to the size of a single cell. On the other hand, a 200 keV photon incident on gold may induce a 119.25 keV K-shell photoelectron, with a range ≈200 μm, sufficient to traverse several cells. An incident photon with $E < E_K$ can instead eject an electron from a shell higher than K-shell (i.e. L, M shells), although the photon mass attenuation and absorption coefficients rapidly become comparable to that of soft tissue at low energies, so that only the inner shells (K, L, M) are potentially capable of producing dose enhancement through photoabsorption (e.g. the mass attenuation coefficient of soft tissue is comparable to gold at energies just below its M-edge, ≈2–3 keV).

Figure 2 presents plots of the mass attenuation and absorption contrast against water for 1% Au ($Z = 79$) or 1% Gd ($Z = 64$), elements commonly used as NREs. Absorption differs from attenuation because above the K-edge, energy transferred from the incident photon to the atom can be converted into fluorescence emission, whereas below the K-edge, characteristic radiation is emitted predominantly via low-energy Auger electrons, which are locally absorbed (see table 1). Byrne *et al* (2017) showed with Monte Carlo (MC) simulations that the enhanced photoelectric absorption contrast against water in a target with 1% atomic gold can not only result in dose enhancement in the target, but can also reduce out-of-target scatter dose. This effect is offset by fluorescence emission and so is most effective for incident x-ray energies below the K-edge.

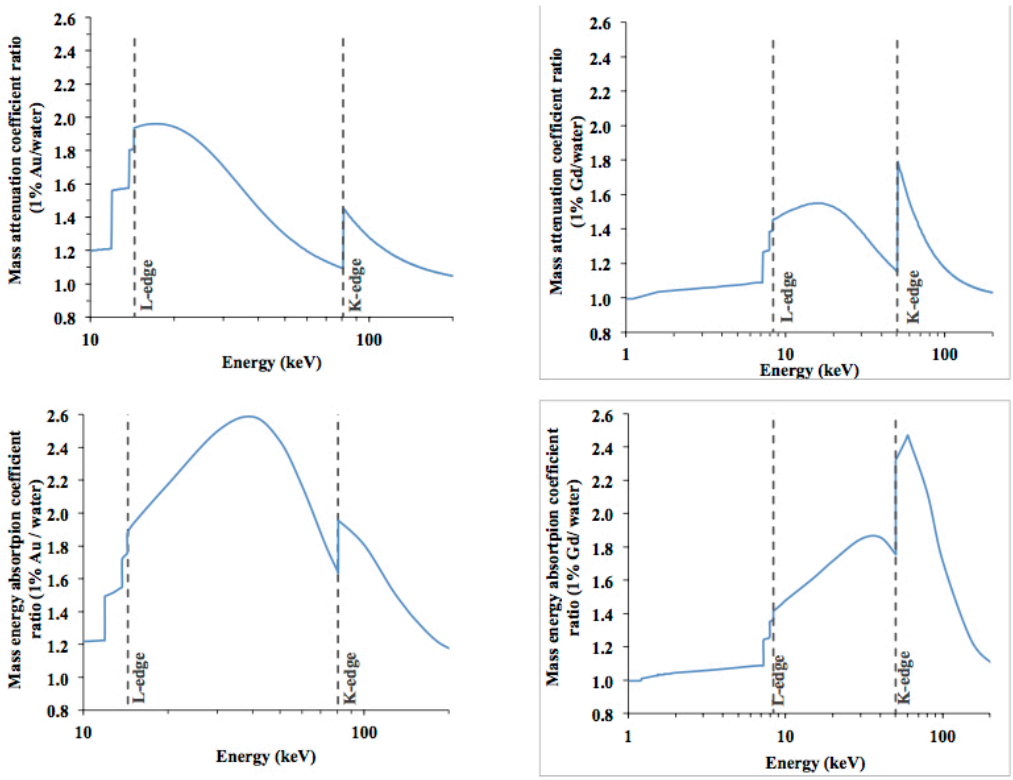

Figure 2. Mass attenuation coefficient (left column) and mass absorption coefficient (right panel) of water containing 1% gold (top row) or gadolinium (bottom row) relative to water only as a function of incident x-ray energy. The *K*-edge and *L*-edge energies of each element are indicated. Data retrieved from NIST/XCOM. Image provided by Byrne, University of Sydney. Reproduced with permission from H Byrne.

Table 1. Total probability of Auger electron emission for *K*, *L* and *M* shell transitions in atoms commonly used as NREs (data from the ENDF flexible database explorer: www-nds.iaea.org/exfor/e4explorer.htm).

	Gd ($Z = 64$) (%)	Hf ($Z = 72$) (%)	Pt ($Z = 78$) (%)	Au ($Z = 79$) (%)
K shell	6.5	4.8	4.2	4.1
L shell	86.2	80.5	75.5	74.6
M shell	99.5	99.1	98.6	98.5

At photon energies >500 keV, Compton scattering becomes the dominant interaction process with high-Z atoms and the atomic cross section varies as $\sigma \propto Z$. At MeV photon energies, pair production can also occur. The atomic cross-section is $\sigma \propto Z^2$, which potentially offers some contrast against water, although pair production is less important than Compton scatter at clinically relevant energies (below 10 MeV).

2.2. Interaction of charged particles with high-*Z* nanoparticles

Particle therapy is a modality that is developing rapidly worldwide (Durante *et al* 2017). The application of NREs to improve particle therapy performance is also progressing rapidly (see the review by Lacombe *et al* (2017)). Charged particles interact with a nanoparticle comprised of high-Z atoms via Coulomb interactions with a cross section that depends primarily on the kinetic energy and charge of the incident particle and on the impact parameter (radial distance from the particle's track to the target). For high-Z targets, nuclear stopping is negligible and fast ions or electrons, typically with energies >1 MeV u^{-1}, lose energy mainly via inelastic Coulomb collisions with the atomic electrons.

The electronic stopping power is mostly due to interactions with outer valence shell electrons until the incident ion or electron energy has sufficiently slowed to energies comparable to the mean orbital energy of inner shell (e.g. *L*, *K*) electrons (Hatano *et al* 2010). An important difference between ions and electrons is their track structure: electrons are readily deflected by collisions, whereas ions, being relatively much heavier, undergo mostly small angle deflections, which gives rise to the characteristic highly localised Bragg peak at the end of their trajectories, with heavier ions (e.g. carbon) exhibiting a more pronounced Bragg peak than protons.

The mass collision stopping power, S, has only a weak logarithmic dependence on Z, with $S \propto -\ln I$ given by the Bethe–Bloch formula, where I is the mean ionisation/excitation potential that generally increases with Z

(Fano 1963). Thus, the mass collision stopping power *decreases* with Z of the target for a given incident charged particle species and energy. For example, gold has $I \approx 790$ eV, which is an order of magnitude larger than that for water $I \approx 75$ eV. This means that radio-enhancement by high-Z nanoparticles exposed to ions or electrons is primarily due to the density contrast of the nanoparticles against tissue. This is different from the case for keV photons, where the contrast against tissue is provided by the strong Z-dependence of photoabsorption (see figure 2). Ions and electrons are nevertheless capable of activating a nonlinear avalanche of electron emission from high-Z nanoparticles through impact ionisation and ensuing Auger cascades. Importantly, the secondary electrons generated by these events can continue to excite and ionise surrounding biomolecules and neighbouring nanoparticles.

Solov'yov and co-workers also proposed that, for ion beam radiation, additional physics may take place that is based on the induction of a propagating shock wave in the medium surrounding a high charge ion track (Verkhovtsev *et al* 2016b). They developed a multiscale model to predict the induction of biodamage due to the combination of multiple mechanisms including shock-induced excitation/ionisation of the medium, transport of secondary particles, chemical interactions, and thermo-mechanical damaging pathways. Although their multiscale model does not explicitly consider nanoparticle radio-enhancement, it does nevertheless consider processes initiated at the nanoscale and thus potentially offers new insights into NRE in the context of ion-induced radiation damage effects.

2.3. De-excitation processes

Following ionisation of an inner shell by either photons or charged particles (electrons or ions), an excited atom can de-excite via fluorescent photon emission or Auger electron emission (Evans 1955). The relative importance of each process depends on the target atomic number Z. For high-Z atomic targets, K-shell de-excitation occurs predominantly via fluorescence emission, e.g. for $Z > 55$, the probability of atomic de-excitation by K-alpha fluorescence is higher than 95%. De-excitation of high-Z atoms via Auger electron emission occurs predominantly from inner shells higher than the K-shell, e.g. for $Z > 60$, the total probability of atomic de-excitation by Auger L shell transitions is 60–80% (see table 1). Note that the Auger process takes place after K shell ionisation and subsequent L shell electron decay into the K shell.

Fluorescent photons generally travel further than Auger electrons and thus delocalise the local perturbation away from a nanoparticle. For gold, for example, the K alpha transition energy is ≈69 keV, corresponding to a photon attenuation length of ≈5 cm in tissue, whereas typical Auger electrons (energies < 100 eV) correspond to a range < 10 nm in tissue. Although the mass collision stopping power of low-energy electrons traversing a high-Z medium is not well known, they may be readily stopped within a high-Z nanoparticle by its high density. Thus, the size of a high-Z nanoparticle determines how many Auger electrons can effectively escape self-absorption (McMahon *et al* 2011a). Similarly, nanoparticle coating can also attenuate Auger electrons that would otherwise contribute to radio-enhancement (Xiao *et al* 2011). For smaller nanoparticles, the chain of escaping multiple low-energy Auger electrons may result in a highly reactive nanoparticle with highly charged atomic states. The nanoparticle atoms, excited by intra-atomic Auger decay, can de-excite via inter-atomic/-molecular electronic decay involving neighbouring water and other biomolecules (Stumpf *et al* 2016). Both inter-atomic Coulomb decay (Jahnke *et al* 2010, Mucke *et al* 2010, Gokhberg *et al* 2014), driven by energy transfer, and electron-transfer mediated decay, driven by charge transfer (Stumpf *et al* 2013), are ultra-fast relaxation processes that may ionise surrounding molecules and produce slow electrons, thereby amplifying radiation damage beyond that predicted by Auger decay alone.

At very low-energies (typically tens of eV), an excited atom can also de-excite via collective transport processes that redistribute energy across electronic states (Fano 1992, Hatano *et al* 2010). Some noble metal atoms such as gold and platinum can de-excite via decay of surface plasmons, resulting from the delocalisation of electronic excitations into coherent motions of valence electrons (Kittel 1963, Verkhovtsev *et al* 2015a, 2015b). Solov'yov and co-workers demonstrated the yield of low-energy ($<$50 eV) electrons can be significantly enhanced, compared to water, by damping of surface plasmons as well as giant atomic resonances in high-Z nanoparticles excited by ion irradiation (Verkhovtsev *et al* 2015a, 2015b). Following an excitation event such as a low-energy Coulomb collision, thermal equilibrium is eventually restored through electron-phonon interactions (Kittel 1963). Equilibrium is also recovered through recombination of thermalised electrons, although sub-excitation electrons can also undergo dissociative electron attachment to surrounding water and other biomolecules, causing further radiation-induced damage (Boudaiffa *et al* 2000, Pan *et al* 2003).

Although a detailed exposition of the physico-chemical stage of radiation-induced effects is beyond the scope of this review, it is important to highlight the critical role that free radicals play in NRE effects. NPs have the capacity to release copious low-energy electrons in nano-scale volumes, which enhances the production of free radicals in the vicinity of the NPs. This high density of radicals can not only create a positive feedback on NP activation, but can also trigger biological signalling pathways that result in enhanced cell death.

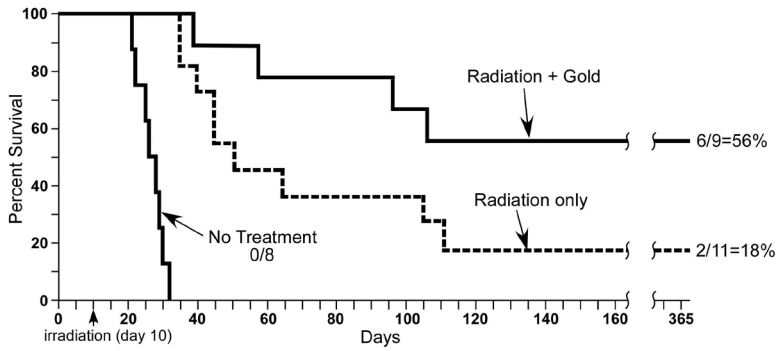

Figure 3. Survival fraction of mice bearing brain tumours after treatment with 35 Gy of 100 kVp radiation plus IV injection of AuNPs ($n = 9$) and treatment with radiation only ($n = 11$), compared to survival without treatment ($n = 8$). Image provided by Hainfeld, Nanoprobes.com. Reproduced with permission from J Hainfeld.

3. *In vivo* studies—proof of concept

The amplification of radiation effects with high-Z compounds was first demonstrated *in vivo* using iodine complexes combined with keV synchrotron x-rays (Adam *et al* 2003). The first proof of concept using nanoparticles as radio-enhancers was demonstrated with gold nanoparticles (AuNPs) activated by keV x-rays (Hainfeld *et al* 2004).

3.1. Gold nanoparticles

Gold nanoparticles (AuNPs) are the most studied NREs owing to their high electronic density, which is favorable to amplification of radiation effects. In addition, small (<20 nm) AuNPs have a relatively straightforward synthesis route, high stability in biocompatible solvents, low toxicity, and also good biodistribution and pharmacokinetics (Perrault *et al* 2009, Laurent *et al* 2016). The effect of AuNPs activated by photons has been expertly reviewed by Butterworth *et al* (2012, 2013) and Jain *et al* (2012) (see also the earlier review by Hainfeld *et al* (2008)) and more recently by Haume *et al* (2016). Here, we summarise major findings in a broader context as well as reviewing more recent studies that have since been published in the literature.

Hainfeld *et al* (2004) were the first to demonstrate the ability of AuNPs to enhance the effect of x-ray radiation. They showed that intravenous injection of 1.9 nm AuNPs (up to 2.7 g Au/kg) improves the survival of mice bearing subcutaneous EMT-6 mammary carcinomas treated with 26 Gy of 250 kVp x-rays. A major breakthrough of this study was the preferential tumour targeting that these small AuNPs exhibited, an important attribute that was not observed in earlier studies (e.g. Herold *et al* (2000)). This was partly attributed to the small AuNP size, which possibly favours enhanced permeability and retention (EPR) through the impaired vasculature structure around tumours (although whether the EPR effect is relevant in humans has been questioned—see e.g. Danhier (2016)). Since this pioneering *in vivo* study, the field has seen a proliferation of other studies that have confirmed the radio-enhancement property of AuNPs.

Continuing on from their pioneering *in vivo* studies, Hainfeld *et al* (2013) studied the image contrast and radiotherapy enhancement effects of 11 nm AuNPs intraveneously injected into mice bearing a highly malignant brain tumor. After delivering 35 Gy of 100 kVp x-rays, they found significant improvement in long-term (>1 year) survival of mice receiving AuNPs (4 g Au/kg) and radiation (≈56%) compared to radiation alone (≈19%) and no treatment (0%) (see figure 3). The radiation dose enhancement factor was estimated to be ≈300%. Although they demonstrated a localization to the brain after injection and observed a 19:1 tumor to normal brain uptake, the majority of AuNPs were blocked by the normal blood-brain barrier. Hainfeld and co-workers took advantage of this accumulation of AuNPs and performed contrast-enhanced, high-resolution imaging of the brain tumor using micro-CT.

CT-guided radiotherapy using AuNPs to enhance both CT image contrast and radiation effects in a tumour was studied by Al Zaki *et al* (2014). They found a 1.7-fold longer median survival time of mice bearing a HT-1080 human fibrosarcoma tumour treated with AuNP-assisted radiotherapy compared with radiotherapy alone (6 Gy at 150 kVp) using 650 mg Au/kg. The NPs consisted of 1.9 nm AuNPs encapsulated within polymeric micelles (hydrodynamic diameter ≈75 nm), which provide longer circulation time, better tumour uptake and more efficient excretion than core AuNP of the same size, as well as rapid clearance and reduced accumulation from the reticuloendothelial system. The high tumour uptake of these NPs resulted in better CT image contrast, thus demonstrating the potential for improving delineation of tumour margins.

In a similar theranostic study, Zhang *et al* (2015) used clusters of 2 nm AuNPs protected by a glutathione shell and also found high uptake in U14 cervical carcinoma bearing mice, as demonstrated by enhanced CT

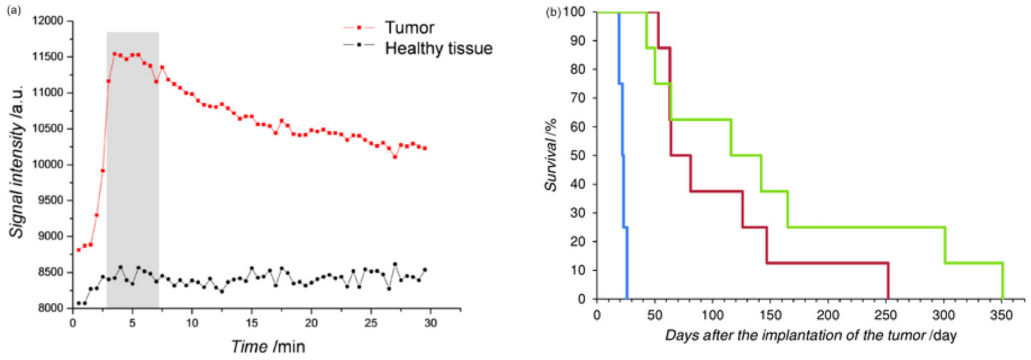

Figure 4. (a) Temporal profile of the the MRI signal intensity in tumour and in healthy tissue in the brain of a 9LGS-bearing rat after IV injection of Gd-chelated AuNPs, with the grey area showing maximal signal contrast; (b) survival curves of 9LGS-bearing rats following treatment with microbeam radiation therapy (MRT) 5 min after IV injection of Gd-chelated AuNPs (green curve, $n = 8$) and treatment with MRT only (red curve, $n = 8$), compared to no treatment (blue curve, $n = 4$). Reprinted with permission from Miladi *et al* (2014). Copyright 2014 John Wiley and Sons, Inc. all rights reserved.

image contrast relative to mice without tumour. They also found a ≈66% decrease in tumour volume following 5 Gy treatment with ^{137}Cs gamma rays with the peptide-protected AuNP clusters, with a concentration of 5.9 mg Au/kg (injected intraperitoneally), compared to radiation only.

A different approach altogether was taken by Kunjachan *et al* (2015), who investigated NP-enhanced radiation damage to the tumour neo-endothelium as a treatment strategy for tumours that otherwise respond poorly to standard therapies. Using PEGylated AuNPs (2–3 nm core, 8–10 nm hydrodynamic diameter), surface functionalised with a neo-vascular targeting ligand, they treated pancreatic tumour xenograft mice with 10 Gy of a 220 kVp x-ray beam. After excising the tumours 24 h after treatment, they found a 3-fold increase in DNA damage compared to control groups.

As pointed out by McQuade *et al* (2015), an important limitation of using AuNPs as a theranostic platform is the significant disparity between the high gold concentration required to enhance CT image contrast (typically of the order of grams Au/kg body weight) compared to the tumour concentration required for radio-enhancement (up to three orders of magnitude lower). McQuade and co-workers instead developed a theranostic approach that uses magnetic resonance (MR) imaging, with contrast enhanced by 14 nm superparamagnetic iron oxide nanoparticles (SPIONs) loaded into pegylated micelles together with 2.2 nm AuNPs (total hydrodynamic diameter ≈100 nm). Similar to the study by Al Zaki *et al* (2014) and McQuade *et al* (2015) demonstrated a radio-enhancement effect of these NPs in HT-1080 tumour-bearing mice treated with 6 Gy of 150 kVp x-rays and 400 mg Au/kg, with a ≈1.5-fold improvement in mean survival of mice treated with AuNP-SPION-loaded micelles compared to radiotherapy only. Additionally, they demonstrated an enhanced contrast of the MR tumour image, confirming tumour uptake of the AuNP-SPION-loaded micelles, and observed a correlation between MRI contrast-enhancement and tumour volume decrease, suggesting contrast-MRI can predict tumour response to treatment.

In a similar rat study, Miladi *et al* (2014) coated ≈2 nm AuNPs with gadolinium chelates to show that MR contrast imaging can be used to optimise tumour radio-enhancement by monitoring the AuNP biodistribution and delaying irradiation until tumour uptake is observed. They found a significant peak in tumour uptake compared to healthy tissue internalisation approximately 5 min after intravenous injection (see figure 4(a)). Using the European Synchrotron to deliver Microbeam Radiation Therapy (MRT—with an x-ray spectrum spanning 50–350 keV), they found a 78% increase in median survival, compared to MRT only, of rats bearing the highly radioresistant 9L gliosarcoma brain tumour when treated with MRT 5 mins after injecting the Gd-chelated AuNPs (0.7 ml with [Au] = 50 mM, corresponding to ~23 mg Au/kg for a 300 g rat) (see figure 4(b)).

More recently, the same team has observed that relatively small changes in the chemical formulation of the macrocyclic chelators used to graft gadolinium complexes on AuNPs can significantly affect the size, biodistribution and pharmacokinetics of AuNPs as well their radio-enhancement effect. They found that ≈2.3 nm AuNPs coated with TADOTAGA–Gd perform the best in improving the life span of 9L gliosarcoma bearing rats treated by kV x-ray MRT owing to their ability to penetrate deeper into the tumour volume (Laurent *et al* 2016).

The studies summarised above used kV x-rays as radiation modality to take advantage of the high photoelectric absorption cross-section and consecutive release of secondary electrons from NREs to amplify radiation effects (see section 2). This physical basis notwithstanding, other recent *in vivo* studies have reported nanoparticle radio-enhancement using higher energy x-rays, including clinical MV beams.

For example, the ≈66% decrease in tumour volume reported by Zhang *et al* (2015) using clusters of 2 nm AuNPs (5.9 mg Au/kg) was achieved using a ^{137}Cs gamma source (which has a spectrum extending from kilovoltage x-rays to gamma-rays, peaking at 662 keV).

Similarly, Su *et al* (2015) delivered 5 Gy with a ^{60}Co source (mean gamma energy 1.25 MeV) to treat tumour-bearing mice injected with AuNPs (≈50 mg Au/kg body weight) conjugated with a tumour-targeting peptide and found more apoptosis and tumour volume reduction compared to radiotherapy using AuNPs without targeting peptides.

Using a clinical 6 MV beam, Wolfe *et al* (2015) investigated the effects of gold nanorods (AuNRs; ≈31 nm × 9 nm) conjugated with a tumour-targeting agent (goserelin) in a mouse prostate cancer model. The relatively high tumour cell accumulation of the AuNRs due to the targeting agent (and also to the EPR effect in rodents), allowed a relatively low concentration of gold to be used effectively (10 mg Au/kg body weight). A biodistribution study showed that the intratumoural accumulation of unconjugated (but pegylated) AuNRs was approximately 3-fold less. Radiotherapy (5 Gy) was delivered 24 h post-injection, and the team found enhancement of MV radiation effects by the goserelin-conjugated AuNRs, as evidenced by reduced tumour growth compared to MV treatment using unconjugated AuNRs and radiotherapy only. They attributed the MV radio-enhancement to clustering of the targeting AuNRs inside the tumour cells and the consequent increase in ionization density within the cytoplasm.

A similar conclusion was drawn by Dou *et al* (2016) who injected tumour-bearing mice with 13 nm pegylated AuNPs (delivering 60 nmol Au/kg, corresponding to just 12 μg Au/kg) and found dramatic inhibition of tumour growth following radiotherapy with clinical 6 MV beam treatment when compared to radiotherapy alone. Moreover, they observed complete eradication of tumour cells when treatment was delivered 4 h post intravenous injection, thus demonstrating again the importance of circulation time. They postulated that smaller AuNPs are more efficient than larger ones because they can form higher density clusters and release more electrons than larger AuNPs.

Popovtzer *et al* (2016) evaluated the efficacy of combined treatment of nanoparticle with radiation to the treatment of head and neck cancer cases. They showed that the treatment of mice with a clinical 6 MV flattening-filter-free (FFF) beam combined with intraveneous injection of 6 mg Au/kg 30 nm AuNPs coated with cetuximab (an inhibitor of the epidermal growth factor receptor which is overexpressed in head and neck and other cancers) resulted in suppressed tumour growth compared to radiation only and radiation with cetuximab. Furthermore, using immunohistological markers, they established that the overall impact of AuNPs is due to a combination of physical radio-enhancement and biological radio-sensitization (in particular enhanced tumour apoptosis) effects.

These *in vivo* studies demonstrated the capacity of AuNPs to enhance the effects of MV beam radiation. This is somewhat unexpected because at these energies, the dominant photon interaction process is Compton scattering. Although the Klein–Nishina electronic cross-section does not explicitly depend on Z, the effective probability of a Compton scatter interaction in the presence of AuNPs may be higher than predicted by the Klein–Nishina differential cross-section because of the availability of multiple nearly-free electrons in the outer shells of many gold atoms per AuNP. The radio-enhancement by AuNPs of gamma and MV photon radiation arises from successive Compton scatter events that not only generate recoil electrons but also degrade photon energy to levels at which the photoelectric effect becomes increasingly more probable. For instance, a photon with an initial energy of 1 MeV is most likely to undergo a small-angle Compton event (as predicted by the Klein–Nishina cross-section), losing a relatively small increment of energy to a recoil electron, after which the photon has a slightly higher probability of scattering through a larger angle and losing more energy. Once a few low-energy recoil electrons are produced, these can also participate in Compton scatter events, potentially creating a cascade of scatter events localised to the NPs. In the case of a clinical MV beam at depth, this localised effect can be enhanced by the spectral component containing unattenuated primary keV photons (especially for a FFF beam), but also by the significant flux of secondary 'contamination' electrons that can ionise NREs multiple times (see figure 5). This creates steep nanoscale gradients in energy deposition in the vicinity of NP clusters, as observed following cellular internalization, due to the effective increase in local density of heavy atoms (Berbeco *et al* 2011, McMahon *et al* 2011b).

Less evidence is available for AuNP radio-enhancement combined with incident proton or heavy ion beams compared to keV x-rays. Kim *et al* (2010) were the first to demonstrate that small (1.9 and 14 nm diameter) AuNPs (and also 13–15 nm SPIONs) enhance the effect of proton irradiation. In their pioneering study, they observed ≈90% and ≈75% volume reduction of CT26 mouse tumours following intravenous injection of AuNPs and SPIONs (100 or 300 mg NP/kg), respectively, and irradiation with a 41.7 MeV spread out Bragg peak (SOBP) beam (see figure 6(a)). Note, however, that relatively high concentrations were injected to achieve these therapeutic effects: 15–55 g Au/kg body weight (and 5 or 15 g Fe/kg body weight). Nevertheless, from consecutive *in vitro* CT26 cell experiments, they established the link between *in vivo* impact and increased cell killing in the presence of NPs. They initially proposed that the observed radio-enhancement is due to particle induced x-ray emission (PIXE), although this is now suggested to play a negligible role in early stage mechanisms (see e.g. Cho *et al* (2016)). Indeed, in a similar follow-up study, Kim *et al* (2012) observed enhanced production of reactive oxygen species (ROS) in cells which they attributed primarily to secondary electron emission from NPs following activation either directly by proton bombardment or indirectly via ROS produced by proton water radiolysis.

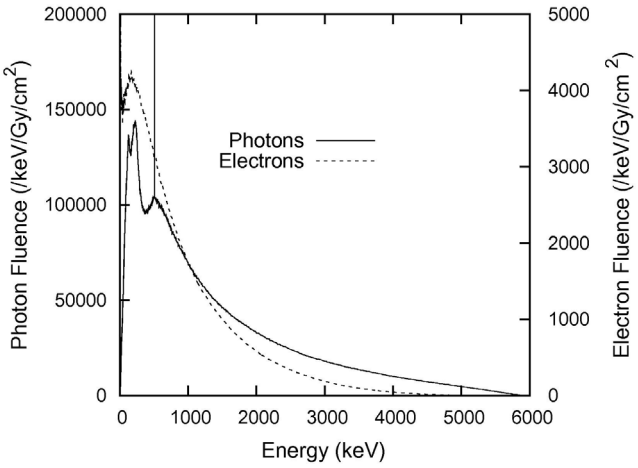

Figure 5. Photon and electron energy spectra at a depth of 5 cm in a cylindrical water volume irradiated with a clinical 6 MV linac beam. Reprinted from McMahon *et al* (2011b). Copyright 2011, with permission from Elsevier.

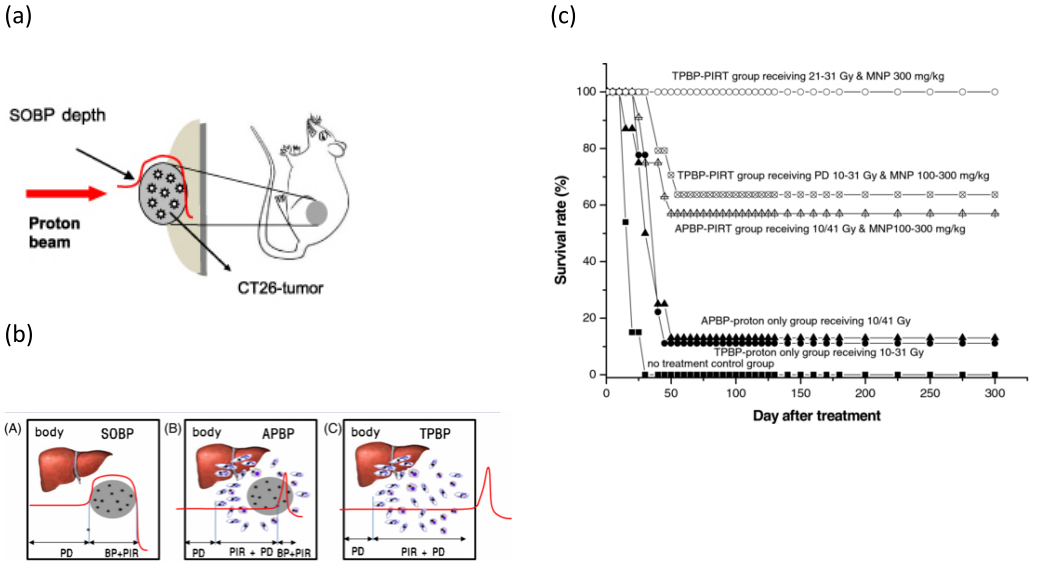

Figure 6. (a) Experimental setup of spread out Bragg peak (SOBP) proton beam irradiation of a CT26 tumour in a mouse (reproduced from Kim *et al* 2010. © IOP Publishing Ltd. All rights reserved.); (b) representations of irradiation conditions (APBP is absorbed pristine Bragg peak and TPBP is traversing pristine Bragg peak); (c) Kaplan–Meier survival curves for various treatments of a CT26 mouse tumour model—filled squares: no radiation treatment ($n = 4$), and AuNP alone (300 mg NP/kg, no radiation; $n = 4$), indistinguishable from no treatment; filled triangles: APBP protons alone (BP dose—41 Gy, $n = 8$); filled circles: TPBP protons alone (10–31 Gy, $n = 9$); open triangles: treatment-Ab (41 Gy, $n = 32$) after IV injection of 100–300 mg/kg FeNP or AuNP; open squares: treatment-Tr (10–31 Gy, $n = 61$) after IV injection of 100–300 mg/kg FeNP or AuNP; and open circles: treatment-Tr (21–31 Gy, $n = 23$) after IV injection of 300 mg kg^{-1} AuNP or FeNP ((b) and (c) Reproduced from Kim *et al* 2012. © 2012 Institute of Physics and Engineering in Medicine. All rights reserved).

Interestingly, they also found that proton and NP treatment of the same tumour in mice was less effective when using the Bragg peak (BP) than when using the traversing beam; complete tumour regression and 100% long-term (1 year) survival was found for the group receiving 31 Gy and 300 mg NP/kg (see figure 6(c)). Note, however, that high Au (and Fe) injected doses were again used, with tumour uptake reported to be 59 mg Au/kg tissue and 41 mg Fe/kg tissue. Despite these high concentrations, no toxicity effects were reported in mice receiving only 300 mg NP/kg body weight treatment, without radiation (see figure 6(c)). To our knowledge, these are the only *in vivo* studies to date that provide evidence of the potential for metal core NREs to improve proton beam treatment. Additional *in vivo* studies are needed to reproduce these results and elucidate the underlying mechanisms responsible for the observed difference in treatment outcomes for the traversing and BP proton beam components.

3.2. Gadolinium-based nanoparticles

Gadolinium (Gd) is a lanthanide commonly used as a magnetic resonance image (MRI) positive contrast agent because of its 7 unpaired electrons in its 4f subshell, which are not involved in bonding when Gd is in its most

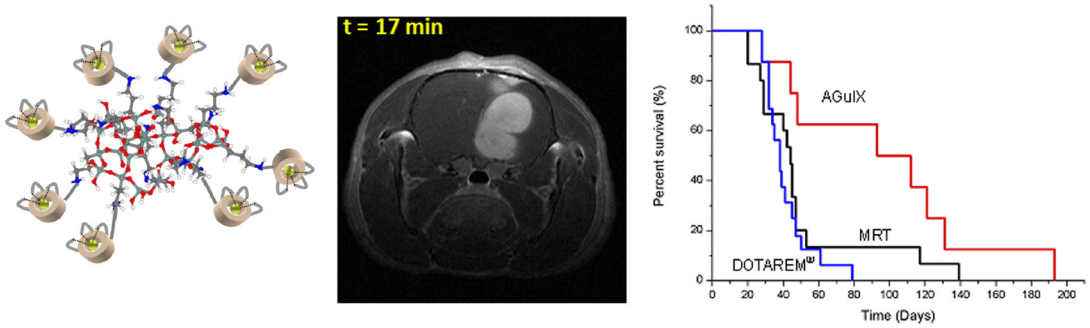

Figure 7. Left—schematic representation of the AGuIX® Gd-based nanoparticle (⩽5 nm size). Green atoms denote the Gd atoms chelated by DOTA derivatives. The polysiloxane matrix is composed mainly of silicon (grey) and oxygen (red). Centre—T1 weighted magnetic resonance image (MRI) of the brain of a 9L gliosarcoma (GS)-bearing rat acquired 17 min after AGuIX® injection, showing tumour contrast enhancement. Right—survival fractions of 9LGS-bearing rats treated only by microbeam radiation therapy (MRT) (black, $n = 15$), by MRT 20 min after injection of DOTAREM® (blue, $n = 16$), and by MRT 20 min after intravenous injection of AGuIX® (red, $n = 8$). Reprinted under CC BY 3.0 from Sancey *et al* (2014).

common oxidation state, Gd^{3+}. With Gd's relatively high atomic number ($Z = 64$) and mass absorption contrast against tissue (see figure 2), the potential radio-enhancing properties of Gd-based nanoparticles (GdNPs) are also being explored (see Sancey *et al* (2014) and Lux *et al* (2015) for reviews). Unlike AuNPs, GdNPs are not metal core nanoparticles but rather compounds usually comprised of Gd chelates with a relatively small number of Gd atoms. Tillement and co-workers carried out a number of studies investigating a new class of ultrasmall (<5 nm hydrodynamic diameter) GdNP, called AGuIX® (manufactured by NH TherAguix, Lyon, France), for MRI-guided radiotherapy. AGuIX® consists of ≈3.0 ± 1.0 nm gadolinium chelates surrounding a polysiloxane core (Bridot *et al* 2007, Mignot *et al* 2013). Tillement and co-workers found that AGuIX was able to cross the blood-brain-barrier in glioma-bearing rats, but not in healthy mice, with a rapid increase in MR signal intensity 1 min after intravenous injection (Le Duc *et al* 2011, Sancey *et al* 2014). The signal remained saturated up to 24 h post-injection of AGuIX® with [Gd] = 40 mM. Enhancement of radiation effects was demonstrated both *in vitro* and *in vivo*. The median survival time of gliosarcoma-bearing rats treated with MRT was found to increase by a factor of ≈2, from 46 d to 96 d, when AGuIX was intraveneously administered 24 h before treatment compared to treatment only, i.e. without AGuIX (Le Duc *et al* 2011, Sancey *et al* 2014) (see figure 7). Similar results were also achieved with kV radiotherapy and AGuIX delivered to mice bearing multiple brain metastases (Kotb *et al* 2016). These treatment outcomes were achieved with milligrams of Gd/kg body mass, which is considerably lower than the typical doses of gold used in previous *in vivo* studies. Indeed, in a follow-up study, Tillement and co-workers obtained x-ray fluorescence maps of 9LGS bearing rat brains after intravenous injection of AGuIX and demonstrated that as little as 15 ppb of Gd in a tumour is sufficient to enhance the efficacy of the treatment (Dufort *et al* 2016).

In a slightly different approach, Detappe *et al* (2016) investigated AGuIX® GdNPs and showed that in addition to enhancing MR image contrast, they also enhanced sensitivity to both pre-clinical kV and clinical MV x-ray beams. In their study, pancreatic tumour-bearing mice were injected with 0.25 mg g^{-1} of the GdNPs and a treatment plan was delivered using a small-animal irradiator (220 kVp beam, 10 Gy) or a clinical linac (6 MV flattening filter free beam, 10 Gy). Significant tumour growth suppression (≈3-fold decrease in tumour volume) and improvement in overall survival (from 45 d to 85 d) was observed for the mice treated with the GdNPs compared to those treated without them using the pre-clinical kV beam. For the clinical MV beam, tumour growth was less suppressed, but tumour volume was still approximately halved compared to treatment without GdNPs and survival was extended by ≈40 d, similar to the pre-clinical kV irradiation results. Similar results were found in a related subsequent study (Detappe *et al* 2017) using AGuIX® complexed with bismuth (Bi), primarily to enable CT contrast imaging.

The effect of GdNPs combined with particle therapy has not yet been demonstrated *in vivo* but promising results have been obtained *in vitro* (see section 5).

3.3. Hafnium and iron oxide based nanoparticles

Radio-enhancement by hafnium ($Z = 72$) oxide (HfO_2) nanoparticles (HfNPs) has been investigated with *in vivo studies* as well as with *in vitro* and simulation studies by Maggiorella *et al* (2012). They used a commercial product, NBTXR3 HfNPs (hydrodynamic diameter ≈50 nm), developed for intratumoural injection (IT). An A673 human sarcoma model was xenografted into mice which then received 15 Gy from a ^{60}Co source, 24 h after IT injection of NBTXR3 (64 mg ml^{-1}; the amount injected was not provided). They found a significant increase in tumour growth inhibition (82%) for mice treated with radiotherapy and NBTXR3 compared to those

receiving radiotherapy only (72%). Furthermore, they also investigated an epithelial tumour model (HCT116) in mice treated with ^{192}Ir brachytherapy with either two doses of 4 Gy or a single dose of 8 Gy, 24 h after IT injection NBTXR3. For both cases, they observed complete tumour remission 20 d post treatment, whereas tumour growth continued in mice that received brachytherapy without NBTXR3. Separate *in vitro* studies showed that the NBTXR3 NPs accumulated inside endosomes within the tumour cells.

Superparamagnetic iron oxide nanoparticles (SPIONs) were investigated by Choi *et al* (2012) for their potential as NREs in photon activation therapy (PAT) with monochromatic synchrotron x-rays. Choi *et al* (2012) treated CT26 tumour-bearing mice with 13 nm SPIONs (100 mg kg^{-1}) 30 min prior to irradiation with 10 Gy synchrotron x-rays at 7.1 keV (just above the Fe *K*-edge). They observed an increase in tumour concentration of magnetite up to 40 μg Fe/g tissue (a contrast ratio of 17 relative to surrounding muscle tissue) and 80% complete tumour regression, with relapse-free survival for up to 6 months, whereas 80% fatality was observed in the control group receiving radiation only. The authors suggest that SPION-PAT offers a potentially effective treatment strategy for superficial tumours. They did not suggest combining this with MRI to develop a theranostic approach, but this seems an obvious direction for further development.

As mentioned in section 3.1, SPIONs were also investigated by Kim *et al* (2012) for their potential as NREs for proton therapy. They found similar results compared to AuNPs when treating CT26 cells and tumour-bearing mice with 300 mg SPIONs/kg body weight followed by 41.7 MeV proton beam radiation (31 Gy); complete tumour regression and 100% long-term (1 year) survival. It is worth re-iterating here that this impressive treatment outcome was achieved using the traversing component of the proton beam, whereas treatment using the BP component was less effective.

3.4. Summary of *in vivo* studies

Table 2 summarises in chronological order *in vivo* studies carried out to date and their key findings. It is evident from this table that the reporting of results is varied, making it difficult to compare and synthesise the findings. Given the unique value of *in vivo* studies in providing direct evidence for the effectiveness of radio-enhancement, we suggest that future studies report a standard set of results. In particular, we recommend experimental protocols that report on survival over tumour regression, as this provides a link to *in vitro* cell survival studies. Protocols should also include a sufficient sample number to allow statistically significant results to be reported, including both the median and mean survival, with variance, as well as fixed-term survival (e.g. 90 d, 6 months, 1 year). Table 2 shows that critical parameters that determine the *in vivo* efficacy of NREs are the administered concentration (e.g. mg Au/kg body weight) and the tumour-to-normal tissue uptake. Hence, these parameters should be explicitly reported in future studies.

4. Molecular scale studies—evidence of elementary processes

The first evidence of molecular scale radio-enhancement was evidenced by Guo and co-workers (Carter *et al* 2007), who conjugated small (≈3 nm) AuNPs to supercoiled plasmid DNA (≈10 AuNP per ≈5600-bp plasmid) (see figure 8) and irradiated with 100 kVp x-rays. They observed enhancement of single and double strand breaks in the presence of AuNPs. More importantly, using a radical scavenger (Tris base) to reduce the diffusion of hydroxyl radicals down to just a few nanometers, they observed a decrease of radio-enhancement effect. With this method they attributed the AuNP-mediated NRE effect to the production of hydroxyl radicals by secondary electrons released in the nano-size volume.

Following a similar experimental protocol, McMahon *et al* (2011c) quantified the effect of AuNPs on plasmid DNA damage induced by kV x-rays. They found that the induction of single strand breaks does not correlate with the variation of energy absorption coefficient, which questions the relation between radio-enhancement and the photo-electric process. Surprisingly, they observed that the damage did not depend on AuNP diameter or on radical scavenging environment (Tris-EDTA). The effect of AuNPs and x-rays on the induction of double strand breaks was not considered here.

Kobayashi *et al* (2002) have pioneered this field and were the first to propose platinum complexes to enhance effects of x-rays. Plasmids were used as nano-bioprobes and the role of water radicals in radio-enhancement (using DMSO as radical scavenger) was evidenced and quantified (see Kobayashi *et al* (2010) for a review).

Later Porcel *et al* (2010) highlighted the capacity of platinum to improve the performance of medical carbon ions (C^{6+}, 276 MeV amu^{-1}) (see figure 9(a)). They used an experimental procedure similar to Kobayashi *et al* (2002) and Carter *et al* (2007) to compare the capacity of platinum complexes and small (3 nm) Pt nanoparticles (PtNPs) to amplify molecular damage, in particular nano-size biodamage. More interestingly Porcel *et al* (2010) attributed the higher NRE observed with PtNPs than with Pt complexes to collective electronic processes that take place in activated nanoparticles only. They also confirmed the key role of water radicals. Porcel *et al* (2012) then found that PtNPs also enhance the effect of He^{2+} (2.3 keV μm^{-1}) and gamma rays (0.2 keV μm^{-1}) to produce nano-size damages with the same efficacy as the carbon ions at the end of the track (100 keV μm^{-1}).

Table 2. Summary of *in vivo* studies, in chronological order, and key results.

Reference and type of study	Type of NRE and administered dose	Type of radiation and delivered dose	Key results
Hainfeld *et al* (2004) Subcutaneous EMT-6 mammary carcinoma in mice	1.9 nm AuNPs 2.7 g Au/kg IV injection (7 mg Au/kg in tumours)	250 kVp x-ray beam, 26 Gy	• High tumour-to-normal tissue uptake ratio (up to 8.6) • 1-year survival fraction improved by factor ≈4.3 over radiotherapy alone
Kim *et al* (2010) CT26 subcutaneous colon cancer in mice	1.9 nm AuNPs and 14 nm ligand-coated AuNPs; 13–15 nm alginate-coated SPIONs 15–55 g Au/kg; 5 and 15 g Fe/kg; IV injections (<1% uptake in tumours)	41.7 MeV protons SOBP, 100 Gy	• Consistent tumour regression with up to 90% volume reduction following proton therapy with either NP; tumour regrowth for proton therapy alone
Le Duc *et al* (2011) 9LGS tumour in rats	<5 nm GdNPs (AGuIX®). Aqueous colloid IV injection: [Gd] = 40 mM, $V = 1.4$ ml; corresponds to ≈29 mg Gd/kg in a ≈300 g rat.	European Synchrotron MRT, 50-350 keV x-rays (mean ≈ 90 keV) Entrance peak dose ≈400 Gy (valley dose ≈20 Gy)	• Median survival time increased by factor 2 for MRT treatment with AGuIX over MRT only • MRI used to optimise treatment outcome by delivering MRT at peak tumour uptake after AGuIX injection (24 h)
Maggiorella *et al* (2012) Xenograft A673 human sarcoma in mice HCT116 epithelial tumour in mice	≈50 nm HfNPs (NBTXR3) 64 mg ml^{-1} IT injection (amount injected not provided)	^{60}Co gammas (mean: 1.25 MeV), 15 Gy (A673 mice) ^{192}Ir brachytherapy: either 2x4 Gy or single 8 Gy fraction (HCT116 mice)	• 10% more tumour growth inhibition than radiotherapy alone (A673 mice) • Complete tumour remission after 20 d, regardless of fractionation; (HCT116 mice)
Choi *et al* (2012) Subcutaneous CT26 in colon cancer in mice	13 nm SPIONs 100 mg NP/kg IV injection; tumour uptake up to 40 mg Fe/kg tissue	7.1 keV monoenergetic x-rays (photon activation therapy—PAT), 10 or 40 Gy	• High tumour-to-normal tissue uptake (up to 17) • 80% complete tumour regression for 10 Gy PAT-SPIONs • 100% complete tumour regression for 40 Gy with both PAT-only and PAT-SPIONs, but achieved earlier with PAT-SPIONs
Kim *et al* (2012) Subcutaneous CT26 colon cancer in mice	5 nm AuNPs and 12 nm ligand-coated AuNPs; 13–15 nm alginate-coated SPIONs 100 or 300 mg NP/kg IV injections (Au and Fe injection doses not provided; tumour uptake 59–203 mg Au/kg tissue and 41–132 mg Fe/kg tissue, which was <1% injected dose)	45 MeV protons: BP, 41 Gy; and traversing beam, 10, 21, 31 Gy	• Significantly greater tumour regression after proton therapy with NPs compared to without NPs • Traversal beam treatment more effective than BP treatment, with complete tumour regression and 100% long-term survival observed for highest NP dose and proton dose (31 Gy)

(*Continued*)

Table 2. (Continued).

Reference and type of study	Type of NRE and administered dose	Type of radiation and delivered dose	Key results
Hainfeld *et al* (2013) Orthotopic brain tumour (Tu-2449) in mice (malignancy similar to human glioma).	11 nm AuNPs 4 g Au/kg IV (tail) injection	100 kVp x-ray beam, 35 Gy	• High tumour-to-normal brain uptake (≈19) • 1 year survival fraction improved by factor ≈3 over radiotherapy alone
Miladi *et al* (2014) and Laurent *et al* (2016) 9L gliosarcoma in rats	2 nm AuNPs, Gd-chelate-coated: Au@DTDTPA-Gd (Miladi *et al*) and Au@TADOTAGA-Gd (Laurent *et al*) 0.7 ml IV injection: [Au] = 50 mM (~23 mg Au/kg)	European Synchrotron MRT, 50-350 keV x-rays (mean ≈ 90 keV). Entrance peak dose ≈400 Gy (valley dose ≈20 Gy)	• Gd-contrast MRI used to monitor uptake of AuNPs to tumour, before delivering MRT • Median survival time increased by factor ≈1.8 (Au@DTDTPA-Gd) and ≈3 (Au@TADOTAGA-Gd) over MRT only
Al Zaki *et al* (2014) Subcutaneous HT1080 human fibrosarcoma tumour in mice	1.9 nm AuNPs encapsulated in polymeric micelles (hydrodynamic diameter ≈75 nm). 650 mg Au/kg IV injection	150 kVp x-ray beam, 6 Gy	• Median survival fraction increased by factor ≈1.7 over radiotherapy only • 90 d survival increased by factor ≈3 over radiotherapy only • Cell survival decrease for $D > 4$ Gy and DER ≈ 1.2 inferred from LQ model D_{37}
McQuade *et al* (2015) Subcutaneous HT1080 human fibrosarcoma tumour in mice	2.2 nm AuNPs and 14 nm SPIONs loaded into pegylated micelles (hydrodynamic diameter ≈100 nm). 400 mg Au/kg IV injection. Au:Fe mass ratio ≈5.5:1	150 kVp x-ray beam, 6 Gy	• Mean survival time increased by factor ≈1.5 over radiotherapy only • 90 d survival increased by factor ≈2.8 over radiotherapy only • MRI contrast confirmed tumour uptake; correlated with tumour volume decrease
Kunjachan *et al.* (2015) Panc-1 pancreatic tumour xenograft in mice	2–3 nm spherical AuNPs, PEGylated and functionalised with neo-vascular targeting ligand (hydrodynamic diameter ≈8–10 nm) 1.2 g Au/kg IV injection	220 kVp x-ray beam, 10 Gy	• H&E staining of excised tumour 24 h after treatment—massive cell death in tumours treated with AuNPs compared to controls • γH2AX staining of excised tumour 24 h after treatment—3-fold increase in DNA damage for AuNP treated tumour compared to controls
Zhang *et al* (2015) Subcutaneous U14 cervical carcinoma in mice	<2 nm Au nanoclusters enclosed by glutathione shell 5.9 mg Au/kg IP injection	^{137}Cs gammas (mean: 662 keV), 5 Gy	• 66% decrease in tumour volume compared to radiotherapy without NPs
Su *et al* (2015) NCI-H466 subcutaneous lung cancer in mice	20 nm peptide-conjugated AuNPs 50 mg Au/kg IV injection	^{60}Co gammas (mean: 1.25 MeV), 5 Gy.	• 53% lower tumour volume growth using NPs with tumour-targeting peptide compared to non-targeting NPs

(*Continued*)

Table 2. (Continued).

Reference and type of study	Type of NRE and administered dose	Type of radiation and delivered dose	Key results
Wolfe *et al* (2015) Xenograft subcutaneous PC3 prostate cancer in mice	31 nm × 9 nm goserelin-conjugated pegylated Au nanorods 10 mg Au/kg IV injection	6 MV clinical beam, 5 Gy.	• 3-fold more accumulation of Au nanorods in tumour when goserelin used • Tumour growth delayed by ≈17 d compared to RT with/without non-targeted Au nanorods
Dou *et al* (2016) Xenograft HeLa human cervical cancer in mice	13 nm pegylated AuNPs 4.7 μg Au/kg IV injection	6 MV clinical beam, 6 Gy	• Tumour growth rate significantly reduced
Popovtzer *et al* (2016) Subcutaneous A431 head and neck squamous cell carcinoma in mice	30 nm AuNPs coated with cetuximab 6 mg Au/kg IV injection	6 MV FFF clinical beam, 25 Gy	• Tumour growth suppressed • Enhanced tumour apoptosis
Detappe *et al* (2016) Xenograft capan-1 pancreatic tumour in mice	4.5 nm SiGdNPs (AGuIX®) 0.25 mg NPs/kg IV injection	220 kVp SARRP pre-clinical beam, 10 Gy; and 6 MV FFF clinical beam, 10 Gy	• Tumour delineated using MRI after GdNP injection • For kVp treatment with GdNPs, ≈3-fold decrease in tumour volume and ≈90% increase in overall survival, compared to without GdNPs • For MV treatment with GdNPs, tumour volume ≈50% smaller and ≈66% increase in overall survival, compared to without GdNPs
Detappe *et al* (2017) Subcutaneous xenograft A549 lung adenocarcinoma in mice	4.5 nm SiBiGdNPs (AGuIX® complexed with Bi) 420 mg NPs/kg dry weight (no other information provided)	6 MV FFF clinical beam, 10 Gy	• MRI used to determine optimal time to deliver radiotherapy (30 mins post-injection, maximal tumour uptake 3.5%) • Significant improvement in tumour growth delay and survival of mice receiving radiation following NP injection compared to radiotherapy alone

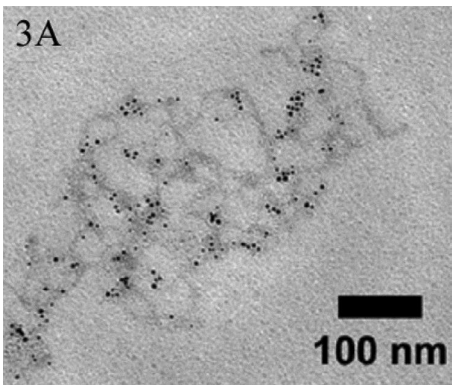

Figure 8. Transmission Electron Microscopy (TEM) image of super-coiled DNA with conjugated gold nanoparticles (≈10 AuNP per plasmid). Reprinted with permission from Carter *et al* (2007). Copyright 2007 American Chemical Society.

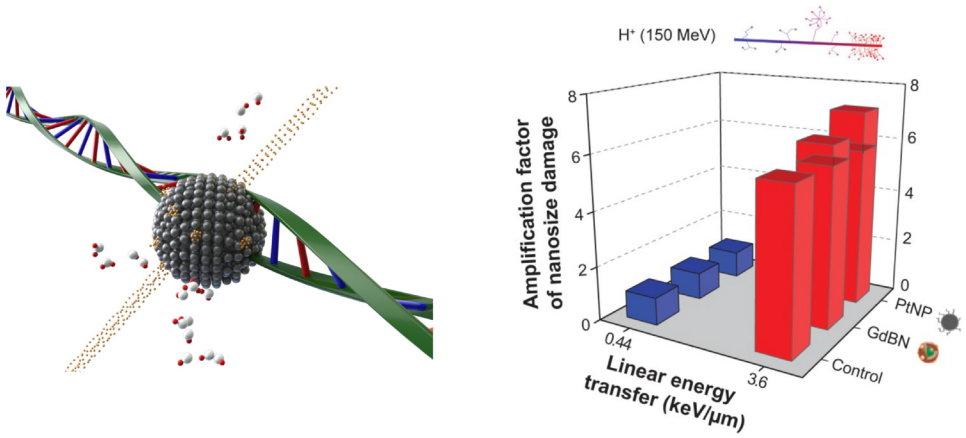

Figure 9. Left—schematic representation of DNA plasmid used as a nano-bioprobe. Image provided by Porcel, University Paris-Sud. Right—amplification factor of nano-size molecular damage induced near the entrance (blue columns) and at the Bragg peak (red columns) of a 150 MeV proton track in the presence of platinum nanoparticles (PtNP) and gadolinium-based nanoparticles (GdBN). Reprinted with permission from Schlatholter *et al* (2016). Copyright 2016 Dove Medical Press.

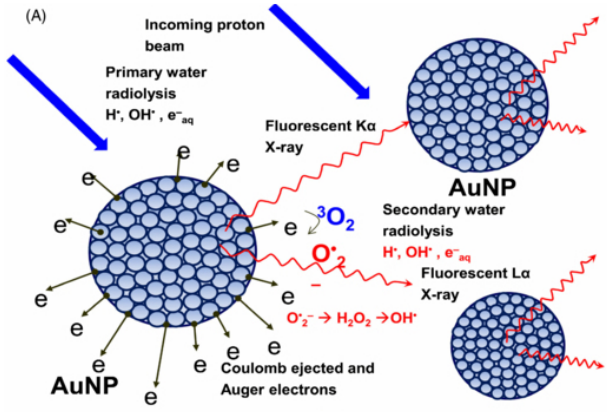

Figure 10. Schematic of early stage mechanisms at the nanoscale including electron emission from gold nanoparticles (AuNP) activated by protons and secondary electrons and photons, and consecutive radical production. Reprinted from Kim *et al* (2012). © 2012 Institute of Physics and Engineering in Medicine. All rights reserved.

In a more recent study, Schlatholter *et al* (2016) compared the molecular effects induced by Pt and Gd nanoparticles activated by 150 MeV protons at the entrance and the end of their track (see figure 9(b)). They found that induction of nano-size damage is amplified by both types of nanoparticles. More importantly, the effect was found to be stronger at the end of the proton track (3.6 keV μm^{-1}). Here again the major role of hydroxyl radicals was evidenced (see figure 10). The enhancement of bio-damage at the end of the proton track is promising for the

use of nanoparticles to concentrate NRE effects in a tumour. Additional *in vitro* and *in vivo* studies are needed to corroborate this result.

It is important to note that DNA plasmids are not representative of nuclear DNA. Rather, they are commonly used as nano-bioprobes to quantify the efficacy of NPs to enhance the induction of complex bio-damage, since double strand breaks are indicative of damages larger than 2 nm (distance between the two strands).

5. *In vitro* studies—cellular impact

NRE effects of NPs has been evidenced *in vivo* by measuring tumour volume, growth rate, and post-treatment survival (section 3). In parallel *in vitro* studies are needed to characterise cellular-scale impact of NRE including cell toxicity, uptake dynamics and radiation-induced cell survival, with the scope to optimise and tailor treatments as summarised below.

5.1. Gold nanoparticles

In vitro studies with AuNPs activated by incident photons have been intensively carried out. Key conclusions are summarised in this section.

Using lipid-encapsulated AuNPs (2.2 nm diameter core) to enhance membrane penetration, Yang *et al* (2014) found greater intracellular spread in melanoma cells than in breast carcinoma cells. Indeed, following irradiation with 4 Gy ^{137}Cs, they observed a 3-fold increase in melanoma cell death in the presence of NPs but no amplification in the breast cancer cell line. They attributed this difference to limited uptake of lipid-encapsulated AuNPs into the cytosol of breast carcinoma cells, as demonstrated by confocal microscopy.

Taggart *et al* (2014) measured cell survival and 53BP1 foci for breast cancer cells (MDA-MB-231), prostate cancer cells (DU-145) and glioma cells (T98G) treated by 225 kVp x-rays. They observed significantly reduced survival of the breast cancer and glioma cells when 1.9 nm AuNPs were present, compared to irradiation without AuNPs. However, no significant AuNP NRE was observed for the prostate cell line. No microscopy was performed in this case, while other studies (e.g. Kong *et al* (2008), Zhang *et al* (2008) and Antosh *et al* (2015)) demonstrated the relation between NRE effects and cellular uptake using AuNPs conjugated with membrane-targeting agents. In Taggart *et al* (2014) the authors obtained DEFs of 1.23 up to 1.90 for the different cell lines incubated with AuNPs. Interestingly, elevated DNA damage, mitochondrial membrane alterations and mitochondrial oxidation were found in all three cells lines exposed to AuNPs, which demonstrated the impact of coating-free AuNPs with biomolecules. Upon irradiation, DNA damage (measured 24 h post-irradiation) and mitochondrial membrane polarisation (measured 1 h post-irradiation) was increased in the breast and prostate cancer cell lines incubated with AuNPs, but not in the glioma cells. Early mitochondrial response to gamma irradiation was also observed by Kam *et al* (2013), who found significant nonlinear changes in the expression of mitochondrially-encoded genes. These results corroborate those of Butterworth *et al* (2013), who surmise that oxidative stress is implicated as the key regulator of radiation damage responses. These studies highlight the important role of mitochondria and the complex nature of biological responses to radiation, a complete understanding of which requires considering the whole cell rather than nuclear DNA only (Kuncic *et al* 2012, Byrne *et al* 2013, McNamara *et al* 2016). This is especially important when considering radio-enhancement by nanoparticles, which generally do not localise to the nucleus.

Currell and co-workers (McQuade *et al* 2016) reached the same conclusion after studying the response of AuNP-loaded cells irradiated with monoenergetic synchrotron x-rays (in the range 8–60 keV) using both clonogenic and DNA damage assays. They found negligible difference in long-term cell killing due to high nanoscale doses when AuNPs were deposited in the nucleus compared to the rest of the cell.

The effect of metal core NPs activated by fast protons has also been studied. In addition to their *in vivo* experiments using a CL29 tumour model and a 41.7 MeV proton beam (see section 3), Kim *et al* (2010) were the first to establish a relation between the localization of NPs (AuNPs and SPIONs) and their impact on cell killing, together with consecutive tumour growth regression. In a follow-up study (Kim *et al* 2012), they also established the major role of reactive oxygen species (ROS) in amplifying cell kill, as illustrated schematically in figure 10. This interpretation of cascade events when metallic based NPs are activated by fast particles is consistent with molecular scale experiments that first demonstrated the proof of principle (see section 4).

The ability of AuNPs (44 nm diameter internalized in phages) to enhance the effects of protons (160 MeV at the SOBP location) was also observed by Polf *et al* (2011) in *in vitro* experiments. They found that the radiobiological effectiveness (RBE) increases by 15% (at SF 10%) to 19% (at SF 50%) for human prostate tumour cells loaded with AuNPs (1 ng Au/cell).

Kirkby and co-workers (Jeynes *et al* 2014) found no statistically significant *in vitro* evidence for NRE effects due to AuNPs (50 nm) activated by 3 MeV protons. Using results from simulation studies, they attributed this to negligible enhancement in secondary electron production from AuNPs for low-energy protons compared to high-energy protons (e.g. 250 MeV). On the contrary, Li and co-workers observed significant amplification of

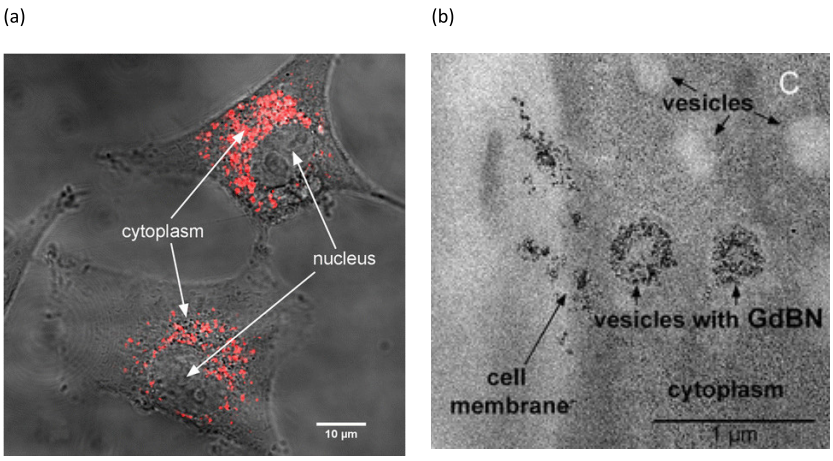

Figure 11. (a) Confocal microscopy image of U87 cells incubated for 12 h with GdNPs-Cy5.5 (red) 0.6 mM; (b) TEM image of U87 cells incubated for 1 h with 1 mM GdNPs. Reprinted under CC BY 4.0 from Stefancikova *et al* (2014).

cell killing with A431 epidermoïd carcinoma cells loaded with PEG coated AuNPs (5 and 10 nm) and treated with 2 MeV protons. Interestingly they highlighted the influence of the beam linear energy transfer (LET). Indeed they observed radio-enhancement with protons of 25 keV · μm^{-1} LET but not with 10 keV · μm^{-1}. Moreover the effect was found to be higher with 5 nm AuNPs. This was attributed to the location of AuNPs in the nucleus, a result that differs from most other AuNP studies (e.g. Kong *et al* (2008), Zhang *et al* (2008) and Antosh *et al* (2015)).

NRE by AuNPs has been demonstrated *in vitro* also using high-energy carbon ions as incident radiation, a modality that is used in particle therapy—also called hadrontherapy—with ions of energies above 200 MeV amu^{-1}. As a first attempt, Kaur *et al* (2013) showed *in vitro* that glucose capped AuNPs (6 nm) enhance HeLa cell killing using 62 MeV carbon ions (290 keV · μm^{-1} LET). They observed a dose enhancement factor (DEF) close to 40% RBE. More recently, a similar result was obtained by Liu *et al* (2015, 2016) with HeLa cells loaded with 15 nm citrate-capped AuNPs irradiated with carbon ions, with cell killing enhancement of ≈25%. The major role of hydroxyl radicals was clearly evidenced using coumarin as a radical marker. As found in other *in vitro* studies, the nanoparticles were located in the cytoplasm.

In summary, small AuNPs (<20 nm) are able to enhance radiation effects *in vitro* when activated by photons and also by charged particles (protons or carbon ions). Their activation depends on the beam characteristics (energy and LET) but the interactions between the beam and AuNPs has not yet been adequately described and simulations are needed to elucidate the effect of ion tracks interacting with NPs.

Apart from AuNPs, several other NREs have been tested *in vitro* as described below.

5.2. Gadolinium-based nanoparticles

Summarised here are studies investigating gadolinium as a NRE, in particular AGuIX®, the Gd-based nanoparticle (GdNP) developed by the group of O. Tillement (University Lyon, France). Irradiation of various cancer cell lines incubated with GdNPs and irradiated by kV and MV photons revealed survival decreased by up to 2.5 times compared to irradiation without NPs (Luchette *et al* 2014, Sancey *et al* 2014, Stefancikova *et al* 2014). Note that GdNPs were found localised in the lysosomes of human glioblastoma cells but not in the nucleus (Stefancikova *et al* 2014) (see figure 11).

Similar results were found using pancreatic cancer cells (Detappe *et al* 2015) and rat glioma cells (Taupin *et al* 2015). In this case, NRE with high-energy photon radiation (gamma-rays and MV beams) was not as strong as with kV x-rays. More importantly, Taupin *et al* (2015) compared the effect of GdNPs (AGuIX®) with a commonly used Gd contrast agent (Magnevist®). They found that both Gd compounds enhanced the cell kill of clonogenic glioma cells treated with 4 Gy x-rays at 65 keV, with maximum enhancement ratios of 2.44 for GdNPs and 1.5 for the Gd contrast agent at the same Gd concentration in the cell culture medium (2.1 mg ml^{-1}). However, only the GdNPs enhanced radiation effects when ^{60}Co gamma rays (mean energy 1.25 MeV) were used as the incident radiation. The authors attributed this difference to the much lower cellular uptake of Gd contrast agent relative to the GdNPs (by a factor ≈30). Interestingly they found that cell cycle and cell proliferation were impacted similarly for all incident photon energies. Last but not least, Stefancikova *et al* (2014) observed that cell killing amplification is not related to nuclear DNA damage, as shown with foci quantification, a result that corroborates previous studies and suggests cytoplasm-driven biological pathways.

The only study reported to date on NRE by GdNPs combined with incident ions is that of Porcel *et al* (2014). They found amplification of radiation effects using carbon ions (150 MeV amu^{-1}, 2.23 keV μm^{-1}) and helium

ions (150 MeV amu^{-1}, 2.23 keV μm^{-1}) used as incident particle beams. The effect was found to be slightly more pronounced with carbon ions (≈19%) compared to helium ions (≈11%). With the use of GdNPs, this study opens up the possibility of nano-theranostics in particle therapy, where GdNPs provide both an NRE effect as well as MRI contrast to monitor the nanoparticle biodistribution and tumour uptake, thereby identifying the optimal time for delivery of the particle beam to maximise therapeutic efficacy.

5.3. Other nanoparticles: platinum, hafnium oxide, iron oxide, cerium oxide nanoparticles, and nanodiamonds

In vitro studies with NREs other than gold and gadolinium are fewer in number and generally less comprehensive. For instance, concentrations used and incubation times are generally not reported.

Pt complexes were one of the first NREs used to amplify the effect of photon or ion irradiation. In particular carboplatin, a chemotherapeutic agent, enhances the production of x-ray-induced strand breaks (Yang *et al* 1995). In contrast, Corde *et al* (2002) did not find any cell killing enhancement when cells were treated with cisplatin prior to x-ray radiation. On the other hand, Usami *et al* (2008) observed a strong cell killing enhancement of mammalian cells treated with terpyridine platine prior to carbon ion and helium ion radiation. This study highlighted for the first time the location of the radio-enhancing agent in the cell cytoplasm.

Molecular scale studies (see section 4) highlighted the radio-enhancement properties of platinum nanoparticles (PtNPs) (Porcel *et al* 2010, 2012), however no cellular scale studies have been carried out. Yet the innate anticancer activity of PtNPs alone has been demonstrated by increased DNA damage and apoptosis associated with genotoxic stress (Asharani *et al* 2010). It has been proposed that the damaging effects of PtNPs may be caused by the release of soluble Pt ion species that form a complex with DNA similar to that of cisplatin (Gehrke *et al* 2011).

Radio-enhancement by hafnium oxide NPs (NBTXR3—Nanobiotix, France) has been demonstrated by Maggiorella *et al* (2012). In addition to *in vivo* studies (see section 2.3), *in vitro* studies were performed with human fibrosarcoma HT1080 cells used as models to investigate the NRE effects of these NPs combined with ^{60}Co gammas and 6 MV x-rays. For both radiation sources, significant amplification of cell killing was found in the presence of NBTXR3. Using an *ex vivo* clonogenic assay with HT1080 cells from an excised xenograft tumour in mice treated with 4 Gy and 8 Gy of ^{60}Co, 24 h after injection of NBTXR3, they found dose enhancement factors exceeding 1.5, relative to tumour cells from mice that received only radiotherapy.

The properties of SPIONs were explored by Choi *et al* (2012) who performed *in vitro* studies in tandem with *in vivo* studies to probe radio-enhancement using monochromatic synchrotron x-rays tuned to just above the Fe *K*-edge (see section 3.3). An MTT assay showed CT26 tumour cell viability significantly reduced (by up to 70%) with increasing SPION concentration when cells were irradiated 24 h after incubation with the SPIONs. Klein *et al* (2014) also investigated enhancement of radiation effects with SPIONs using different cell lines (tumour and healthy). However, their study focused on the enhancement of ROS production resulting from the interactions of low-energy x-rays with the ligands used to coat the SPIONs, rather than the interaction of the radiation with the high-Z magnetite core, which was not addressed. Interestingly, they observed faster uptake dynamics of SPIONs in tumour cells than in healthy cells, which they attributed to the relatively higher metabolic activity of tumour cells.

Another oxide nanoparticle, comprised of CeO_2, is particularly interesting because it exhibits dual radio-enhancement and radioprotection properties. Previous studies revealed CeO_2 NPs to be differentially toxic to cancer cells and to provide protection to normal cells by capturing reactive oxygen species, thus making them ideal for optimising therapeutic efficacy (see review by Gao *et al* (2014)). Briggs *et al* (2013) showed that CeO_2 NPs are also effective NREs, due to the relatively high atomic number of Ce ($Z = 58$). They found significant effects in survival of radioresistant 9L cells upon treatment with CeO_2 NPs and either 10 MV or 150 kVp x-ray beams, with more lethal effects observed for the kVp x-rays. Subsequent simulation studies have also been carried out by this group to investigate the potential for CeO_2 NPs to enhance proton therapy (McKinnon *et al* 2016).

Lastly, an alternative strategy has been proposed by Grall *et al* (2015) who explored the capacity of hydrogenated nanodiamonds (NDs) to enhance radiation effects. Contrary to other NREs reviewed here, NDs do not posses high-Z elements. Nevertheless, hydrogenated NDs exhibit NRE properties due to their semi-conductor behaviour and negative electron affinity, which are conducive to photo-induced emission of low-energy electrons from their surface (electrons can escape once excited into the conduction band). *In vitro* studies by Grall *et al* revealed enhanced double strand breaks and cellular senescence in different radioresistant cancer cell lines treated with hydrogenated NDs and gamma rays (^{137}Cs, 4 Gy). Interestingly, enhanced production of reactive oxygen species was also found, similar to high-Z NREs.

6. Modelling studies

Different models developed for understanding the impact of radiation on biological systems have been adapted to describe the impact of nanoparticles. Most of these models are based on Monte Carlo simulations. Monte

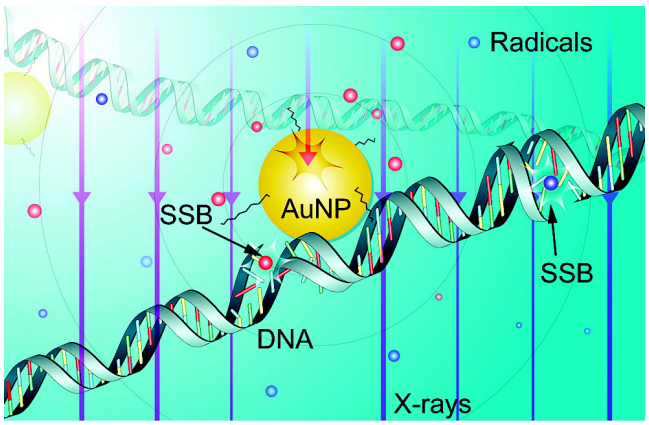

Figure 12. Schematic illustration depicting nanoscale energy deposition enhanced by a ≈3 nm AuNP (AuNP) in close proximity to DNA irradiated by 100 kVp x-rays: the incident x-rays ionise water molecules to produce a uniform distribution of radicals (blue spheres), while secondary electrons (including Auger electrons and photoelectrons) originating from the AuNP produce a higher density of radicals concentrated near the nanoparticle (red spheres). Radicals generated within ≈0.5 nm of the DNA can cause a single-strand break (SSB) with ≈25% efficiency. Trajectories of electrons are not shown, and only the relative average density of radicals generated from these electrons is displayed. Reprinted with permission from Carter *et al* (2007). Copyright 2007 American Chemical Society.

Carlo (MC) particle simulations can be used to model the physical and physico-chemical processes of radiation interactions with biological targets, but cannot be used to study radio-enhancement effects because the biological outcomes cannot be directly simulated (Kuncic 2015). However, MC-based models have been developed which integrate MC simulations with mathematical radiobiological modeling (e.g. McMahon *et al* (2011a) and Lechtman *et al* (2013)). Other modeling approaches have been developed to address the multiscale aspects of radiation damage effects, to better integrate the effect of oxygen in tumour (oxic and anoxic situations), and to bring new understanding when photons or fast ions are used as ionising radiation. Verkhovtsev *et al* (2016a) present a comprehensive overview of theoretical and computational studies of physical phenomena arising from photon, electron and ion collisions with nanoparticles.

6.1. Photon radiation

Stand-alone MC models have proven useful for providing valuable insights into the relevant importance of primary photon and secondary electron processes and calculating nanoparticle-induced enhancement in dose and ionisations for a range of parameters (e.g. target geometry, nanoparticle size and distribution, radiation source energy), which would otherwise be difficult and in most cases impractical to measure experimentally. The first MC studies to investigate dose enhancement by high-Z atoms were carried out by Robar *et al* (2002) for gadolinium and iodine contrast agents and MV photon beams. For Gd, their results predicted significantly more enhancement for a FFF beam (≈11% for 6 MV) compared to a flattened beam due to the additional low energy photons in the FFF beam spectrum.

The MC study by Cho (2005) was the first to investigate dose enhancement by AuNPs for typical MV treatment beams, finding less than 1% enhancement. Carter *et al* (2007), investigated specifically the low-energy electrons released by AuNPs upon kV irradiation, and the ensuing nanoscale energy deposition distribution. They carried out MC simulations to complement their DNA plasmid experiments (see section 4) and concluded that AuNPs need to be located in close proximity to DNA to maximize tumour cell kill by free radicals generated by the low-energy electrons (see figure 12). A number of subsequent MC studies then focused on different kV sources and sizes of AuNPs and their effect on the characteristics of low-energy electrons produced (Cho *et al* 2009, Lechtman *et al* 2011, Leung *et al* 2011, McMahon *et al* 2011a). Lechtman *et al* (2011) also investigated the effects for a clinical 6 MV source compared to a range of kV sources and found that significant cross-firing occurs due to energetic photoelectrons, implying that AuNPs could potentially enhance radiation damage effects even without localising into all tumour cells. They concluded, however, that AuNP radiosensitisation using a 6 MV source is not clinically feasible because of the unacceptably high concentration of AuNP required (approximately 1600 mg g^{-1} tumour is needed to double a prescribed dose of 2 Gy). On the other hand, the MC studies by Berbeco *et al* (2011) and McMahon *et al* (2011b) demonstrated that inhomogeneous accumulation (i.e. clustering) of AuNPs results in steep nanoscale dose gradients that can also arise for a clinical MV source due to the low-energy component of the spectrum (see figure 5).

Douglass *et al* (2013) developed a sophisticated 3D randomized cell model geometry which they incorporated into Geant4 to investigate dose enhancement resulting from AuNP clusters randomly positioned inside the compartmentalized cells irradiated with both 80 kVp and 6 MV x-ray beams. In particular, they were able to

study the effect of Auger electrons by activating and de-activating atomic de-excitation processes in Geant4. They showed that the Auger electrons, by virtue of their very low energies, have a negligible effect on dose enhancement within a cell, and that dose enhancement depends on the location, as well as the size, of the AuNP cluster, with AuNP clusters attached to the cell nucleus resulting in a larger enhancement compared to clusters located in the cytosol or membrane.

Brivio *et al* (2015) adopted the approach of modelling a realistic clinical kV treatment scenario, radiosurgery with AuNPs for neovascular age-related macular degeneration. Here, a 4 mm diameter 100 kVp beam is aimed at the macula to deliver a single ablative dose. The MC model, developed using MCNP6, investigated dose enhancement by AuNPs to the diseased macular endothelial cells. For 20 nm diameter AuNPs of concentration 32 g kg^{-1}, the model predicted a dose enhancement factor of nearly 2, implying significantly reduced risk to surrounding critical organs (i.e. retina/optic nerve) as a result of requiring less radiation dose to achieve the same outcome as treatment without AuNPs.

Given that experimental *in vitro* studies show that NPs tend to localise in the cytosol or organelles other than the nucleus (see section 5), McNamara *et al* (2016) carried out a Geant4 study with a realistic compartmentalised cell model based on measurements of the chemical composition of a lymphocytic JURKAT cell, including separate composition measurements of the nucleus and mitochondrion. They found that the presence of 1% gold in the cytosol, to represent AuNP uptake, increases energy deposition by ≈1.8% due to the additional photoelectrons. Moreover, the dose enhancement is greater in the mitochondrial volumes than in the nuclear volume due to the larger surface area to volume ratio of the mitochondrion compared to the nucleus. These results demonstrate that physical dose enhancement effects in cells are not restricted to the vicinity of NPs and also point to the mitochondria, and mitochondrial DNA, as being viable radiation targets (see also preliminary follow-up simulation studies by McMahon *et al* (2017)).

In another Geant4 study, Zygmanski *et al* (2013) addressed the several orders of magnitude difference in scale between clinically relevant macroscopic dose and the nanoscale transport processes that occur in the immediate vicinity of irradiated AuNPs. They analysed the transition in phase space from macro- to micro-beams incident on AuNPs and investigated the influence of micron-scale source-target geometry, including beam size and AuNP clustering, using both monoenergetic (11 keV–1 MeV) and spectral (50 kVp) x-ray sources. They found both the magnitude and spatial distribution of dose enhancement exhibits a strong nonlinear dependence on AuNP cluster size, thus demonstrating that MC simulation results for dose enhancement due to single AuNPs and specific source-target geometries cannot be simply extrapolated or scaled-up from nanoscales to micron-scales. However, the density and size of nanoparticles are also important because they determine the escape probability of secondary electrons and hence, the dose enhancement in surrounding biological tissue (see e.g. Lechtman *et al* (2011) and McMahon *et al* (2016)).

Owing to the disproportionately large number of studies to date, AuNPs now present a useful benchmark for other NREs. In a comprehensive modeling study, McMahon *et al* (2016) compared the macroscopic and nanoscale effects resulting from nanoparticle-radiation interactions for a range of high-Z elements, including gold, irradiated by kV x-rays just above the K-edge of each material and also a 6 MV linac beam. MC simulations using Geant4 showed that electron impact emission dominates in the case of MV beam irradiation while Auger electron emission dominates in the immediate vicinity of a high-Z nanoparticle irradiated with kV x-rays. A mathematical radiobiological model developed specifically for nanoscale effective dose deposition following kV exposure of high-Z nanoparticles (McMahon *et al* 2011a) was then applied and predicted an optimal radiobiological effectiveness for $Z \approx 34$ and $Z \approx 68$, corresponding to elements at or near germanium and gadolinium.

Edouard *et al* (2010) performed a MC study using MCNPX to compare dose enhancement by iodine, gadolinium and gold contrast media commonly used in synchrotron stereotactic radiotherapy. Using a head phantom model based on clinical CT scans, they considered different x-ray beam qualities, including monochromatic synchrotron x-rays, kVp x-ray beams and a 6 MV linac beam. Their simulations predicted dose enhancement factors in the range of 2–2.4 for all three contrast agents with concentration of 10 mg ml^{-1} using monochromatic synchrotron 40–90 keV x-rays. Slightly lower enhancement factors, but still near 2, were predicted for kV beams with energies 80–120 kVp. For a 6 MV linac beam, a negligible dose enhancement was predicted for all the contrast agents. Another contrast-enhanced radiotherapy simulation study was carried out by Garnica-Garza (2011) using PENELOPE for a pancreatic tumour model. The results predicted that 0.75 mg g^{-1} of Gd distributed uniformly in surrounding healthy tissue could be well tolerated following treatment with a 220 kVp beam, and that with 5 mg g^{-1} Gd delivered to the tumour, produces corresponding treatment plans with excellent dose-volume histograms with sparing of organs at risk and dose delivered to 100% of the tumour volume for 72 Gy.

6.2. Proton and ion radiation

Modeling studies of incident protons radiation effects with AuNPs were carried out by Lin *et al* (2014, 2015). Using TOPAS (TOol for PArticle Simulation, Perl *et al* 2012), a software platform employing Geant4 as the MC

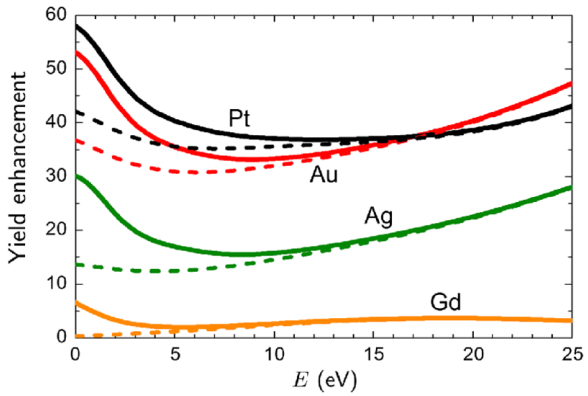

Figure 13. Electron yield enhancement from 1 nm metallic NPs irradiated with 1 MeV protons. *E* is kinetic energy. Dashed lines show the contribution of individual atomic excitations. Solid lines show the resulting contribution, taking into account the contribution from plasmons. Reprinted with permission from Verkhovtsev *et al* (2015a). Copyright 2015 American Physical Society.

engine. They predicted significant dose enhancement in the immediate vicinity of the surface of AuNPs activated by incident protons, at a level comparable to the nanoscale dose enhancement produced for incident kV and MV photons. However, they found that unlike incident photons, which can also produce photoelectrons with a much longer range (typically a few microns), incident protons only produce short-range secondary electrons from collisions with AuNPs and thus, cannot generate dose enhancement on larger scales (Lin *et al* 2014). This was confirmed by another study using TOPAS together with experimental measurements (Cho *et al* 2016). This implies that AuNPs would be required to internalise inside cells and ideally, inside the nucleus to maximize radio-enhancement of protons. In their follow-up radiobiological modelling study, Lin *et al* (2015) predicted that if AuNPs cannot be internalised into tumour cells, then no sensitisation will be observed for proton therapy treatment.

Wälzlein *et al* (2014) were the first to study the relative radiation enhancement effects of different high-*Z* elements, namely gold, platinum, gadolinium, silver and iron. They used the track structure MC code TRAX to evaluate the participation of Auger electrons when NPs of different sizes (r = 22 and 2 nm) are activated by monoenergetic proton beams with energies of therapeutic interest (2, 80 and 300 MeV). They concluded that high-Z metallic nanoparticles may be of great interest to improve proton and heavy ion therapy. Verkhovtsev *et al* (2015a, 2015b) then demonstrated, with theoretical and quantum chemistry calculations using time-dependent density functional theory (DFT), that 1 MeV protons interacting with metallic clusters (3–40 atoms) may induce giant electronic excitations in the metallic atoms due to the ionisation of 5d electrons from outer shells, but also due to excitation of plasmons (collective modes of conduction band electrons). Hence, by evaluating the contribution of each mechanism they found that radio-enhancement by platinum is more efficient than gold, and both are expected to be an order of magnitude more efficient than silver and gadolinium (figure 13). Thus, they established that collective excitation followed by plasmon damping makes a non-negligible contribution to low energy electron emission in the vicinity of metallic nanoparticles (this is relevant for NPs composed of a metallic core, such as platinum and gold NPs, but not for oxides such as Gd-based complexes).

McKinnon *et al* (2016) used Geant4-DNA to investigate local dose enhancement from 100 nm ceramic oxide NPs (Ta_2O_5 and CeO_2) irradiated by 5 MeV and 50 MeV monoenergetic protons. They found that although Auger electrons make a non-negligible contribution to radio-enhancement, it is minor compared to delta electrons produced by impact ionization. They also found a smaller dose enhancement for ceramic oxide NPs ($\approx$1.15) compared to AuNPs ($\approx$1.25) for the same simulation set-up, which they attributed to lower densities. Martinez-Rovira and Prezado (2015) used Geant-DNA to simulate the effects of Au and Gd NPs of sizes ranging from 4 to 50 nm activated by different proton beam configurations (with various distances between the source and nanoparticle and using different source sizes) and found that geometrical parameters (source-target distance in particular) strongly influence the radio-enhancement properties of nanoparticles. In particular, they found a maximum amplification of 1.7 when the distance between the beam and the nanoparticle is zero (which corresponds to the configuration used in the studies of Verkhovtsev *et al* (2015a, 2015b) and Wälzlein *et al* (2014) cited above). On the basis of their Geant4-DNA results, Martinez-Rovira and Prezado concluded that physical processes play a minor role in nanoparticle radio-enhancement in a realistic proton therapy treatment scenario and that consequently, NRE effects observed in experimental studies must instead be largely due to chemical and biological effects (i.e. sensitisation).

However, MC studies to date have not explicitly considered LET effects, which *in vitro* studies have shown to be important (see section 5). Simulations are needed to compare NP activation by heavy ions (e.g. helium and carbon) to NP activation by protons within the Bragg peak. Additionally, simulation studies have not modelled electron transfer effects (Stumpf *et al* 2013) that can potentially contribute to NRE effects beyond that predicted by Auger electron decay and impact ionisation (see section 2.3). MC studies are also needed to simulate the effects of nanoparticle clustering observed in *in vitro* studies. It is likely that strong nonlinear amplification of nanoscale radio-enhancement may result from multi-NP activation by electrons and radicals (see figure 10), yet this remains to be quantified.

7. Opportunities

Emerging opportunities in nanoparticle-enhanced radiation therapy include: (i) image-guided external beam radiotherapy; (ii) internal radionuclide targeted therapy and diagnostic imaging (theranostics); and (iii) concomitant therapies.

7.1. Image-guided external beam radiotherapy

Image guidance is now regarded as essential in external beam radiotherapy. In particular the use of MRI to gain anatomical information without exposure to x-ray CT is a growing trend (Chetty *et al* 2015). Hence, an increasing number of studies focus on GdNPs, which offer the advantage of providing both MRI bright contrast enhancement and radio-enhancement (Le Duc *et al* 2011, Sancey *et al* 2014, Lux *et al* 2015, Taupin *et al* 2015, Detappe *et al* 2015, 2016, Dufort *et al* 2016). An additional advantage is that gadolinium is able to pass the blood-brain barrier and thus, the potential to treat brain tumours with highly targeted radiotherapy is a particularly attractive clinical goal (Kotb *et al* 2016).

Studies to date have demonstrated radio-enhancement effects for a range of incident photons, including kV beams and synchrotron microbeams, as well as clinical MV beams. Similarly, more recent studies have also begun to investigate the radio-enhancement properties of superparamagnetic iron oxide nanoparticles (SPIONs), which are commonly used to enhance dark contrast in MRI (e.g. Huang *et al* (2010) and Khoei *et al* (2014)). While most of these studies have also confirmed the MRI contrast enhancement by Gd-based nano-complexes or SPIONs, to date none have demonstrated enhanced MRI contrast and radio-enhancement *simultaneously*. This is a unique opportunity for MRI-guided external beam radiotherapy.

NREs that can also be imaged provide the added advantage of monitoring their biodistribution and delivering radiation therapy only when peak uptake in the tumour is observed. As mentioned in section 3, pre-clinical animal studies using NREs to enhance CT or MRI contrast in conjunction with radiotherapy has already been demonstrated. X-ray fluorescence (XRF) computed tomography is another modality that has been demonstrated to be useful for imaging AuNP biodistribution in small animals (e.g. Manohar *et al* (2016)). For clinical applications, however, the biodistribution of NREs in the body is needed. While high-Z NREs (e.g. AuNPs) can be monitored by CT imaging, the concentrations that are needed make this modality clinically impractical. Magnetic NREs (e.g. GdNPs, SPIONs), on the other hand, provide MRI contrast even at relatively low concentrations. The potential for theranostic NREs to improve the performance of particle therapy (proton and hadron therapy) remains to be explored.

7.2. Internal radionuclide theranostics

A rapidly emerging branch of nanomedicine is 'radio-nanomedicine', where radio-labeled nanoparticles deliver diagnostic and therapeutic isotopes directly to a tumour. Systemic radiation treatment offers a promising new window of opportunity for tumour targeting, with a minimal exposure of normal tissue that cannot be matched by existing external beam radiotherapy techniques (Zhang *et al* 2010, Lee *et al* 2015).

Initial studies explored labeling nanoparticles with radio-tracers for biodistribution imaging studies with PET or SPECT (de Barros *et al* 2012, Thorek *et al* 2014, Normandin *et al* 2015). This has inevitably led to labeling nanoparticles with radiotherapeutic isotopes. Yook *et al* (2015), for example, conjugated AuNPs with the β^--emitter ^{177}Lu and with the human monoclonal antibody panitumumab specific to the epidermal growth factor receptor (EGFR) that is over-expressed in breast cancer. Their *in vitro* studies showed that even though the antibody targeting agent was effective in promoting cellular internalization of the AuNPs and delivering radiation dose to the nucleus, cross-fire of the β-particles (which have a range $\approx$2 mm in tissue) also contributes to radiotoxicity in neighbouring tumour cells, even without active targeting. This demonstrates an important advantage of internal radiotherapeutic nano-delivery over chemotherapeutic nano-delivery, which requires the drug to be delivered across both the plasma membrane and ideally also the nuclear membrane to achieve maximal efficacy. Radio-enhancement due to the interaction of the emitted particles (alphas, betas, gammas) with AuNPs (or other high-Z NPs) has not been investigated.

7.3. Concomitant therapies

In current clinical practice, radiotherapy treatment is often delivered concurrently with chemotherapy as this has been demonstrated in many cases to be more effective than single-modality treatment (Seiwert *et al* 2007). Considerable research effort has been invested in developing nanoparticle carriers of systemically applied chemotherapeutic drugs to improve targeted delivery to the tumour, both spatially (tumour accumulation, tumour-to-organ ratio) and temporally (circulation time, tumour residence time) but arguably the most promising results have been demonstrated when combined with radiotherapy (Lammers *et al* 2008). Recently, Li *et al* (2016) investigated pegylated AuNPs co-loaded into a hydrogel with doxorubicin (DOX) to achieve combined nanoparticle radio-enhancement and controlled DOX delivery in chemoradiotherapy. They showed, with *in vitro* studies, that tumour cell viability was substantially compromised following 6 MV irradiation when both AuNP and DOX were administered compared to irradiation only or irradiation with AuNPs. With an *in vivo* study, they found enhanced inhibition of tumour cell growth and proliferation after 6 MV radiotherapy treatment with both AuNP and DOX, compared to radiotherapy only, radiotherapy with DOX or radiotherapy with AuNPs. These results suggest that AuNPs play a key role in the synergistic enhancement of chemoradiotherapy treatment efficacy.

An important advantage of concomitant therapies is that they can reduce the amount of NREs needed to achieve improved therapeutic outcomes. In Hainfeld *et al*'s original study in 2004, 2.7 g Au/kg body mass was needed for radio-enhancement. This is not clinically viable for human use and alternate strategies such as combined therapies need to be explored before AuNPs can be clinically translated (Cooper *et al* 2014). In a later study, Hainfeld and co-workers investigated the synergistic therapeutic effects of combined hyperthermia and radiotherapy using AuNP aggregates engineered for infrared absorption (Hainfeld *et al* 2014). They found that the dose required to control 50% of the tumours in mice could be reduced from ≈55 Gy down to <15 Gy using 100 kVp x-rays when combined with hyperthermia.

Radioimmunotherapy is another emerging synergistic approach that is showing enormous promise. In particular, pre-clinical animal studies using checkpoint inhibitors that activate and harness the body's own immune system to fight against tumour cells have shown remarkable improvements in survival when combined with external beam radiotherapy. Importantly, the observed strong response to radioimmunotherapy was replicated in a clinical trial involving patients with different cancer types (Twyman-Saint Victor *et al* 2015). The role of nanoparticle radio-enhancement in radioimmunotherapy remains unexplored.

8. Conclusions and outlook

Several conclusions can be drawn from the results obtained with different high-*Z* NREs (AuNPs, GdNPs, PtNPs, HfNPs and SPIONs). Firstly, *in vivo* small animal studies have provided unequivocal evidence for nanoparticle-mediated enhancement of radiation damage initiated by photons. For incident keV x-rays and MeV gamma rays, radio-enhancement effects generally translate to amplification of radiation damage by a factor of ≈1.5–2 for injected doses <1 g of high-*Z* element per kg body weight. Corresponding *in vitro* studies have produced similar results. For clinically relevant MV photon beams, however, more *in vivo* data (especially statistical survival data) is needed to better quantify possible radio-enhancement effects from NREs. From the perspective of clinical translation, NRE treatment strategies should be evaluated not only in terms of radio-enhancement efficiency, but also in terms of reproducibility and mode of administration, as well as targeting and image guidance capability (to optimise therapeutic gain from NREs by monitoring nanoparticle biodistribution and delivering radiotherapy only when tumour uptake peaks).

The experimental results performed to date verify the underlying principle that NREs have the capacity to transfer energy from incident photons to the surrounding biological medium much more effectively than water molecules, and thus to increase lethality of radiation effects. However, the evidence for NREs activated by protons and heavy ions is considerably weaker; to date, only two *in vivo* studies, conducted by the same group, have been reported for proton beams (and none for ion beams). Additional *in vivo* studies are thus urgently needed to evaluate the relative enhancement of high-LET over low-LET particles, as well as the overall enhancement relative to NREs activated by photons. Here, complementary MC simulations will be invaluable for quantifying relative NRE effects and elucidating the contribution from ion tracks interacting with high-*Z* nanoparticles.

From the *in vitro* studies, we can conclude that nuclear DNA is not an exclusive radiation target and that NRE effects are concomitant with enhanced free radical production when radiation is delivered under normoxic conditions. Here, additional studies are needed to investigate the influence of oxygen concentration on the capacity for NREs to enhance radiation damage in radioresistant hypoxic tumours.

Future *in silico* studies should be carefully designed to complement *in vivo, in vitro* and/or molecular studies and simulate experimental observations (e.g. nanoparticle clustering). Additional physical and chemical processes (e.g. plasmon decay, charge transfer, radical production, oxygenation, recombination and diffusion) also

need to be modelled to clearly identify the key physico-chemical processes, which are otherwise difficult to disentangle and isolate from the biological processes in real experiments.

Lastly, we highlight two emerging paradigms as an outlook for future research. The first is radio-nanomedicine, where radiolabelled high-Z nanoparticles are used to deliver internal radiation therapy. The potential to amplify radiation effects with this approach, in direct analogy to external beam radiotherapy, has not yet been explored. The second emerging opportunity is the development of ultra-high dose rate radiation sources, which demonstrate superior therapeutic index over conventional radiotherapy (Favaudon *et al* 2014, Fouillade *et al* 2017, Montay-Gruel *et al* 2017). To this end, the combination of NREs with new radiation modalities (internal and ultra-high dose rate radiation) opens up a wider range of possibilities for novel nano-enhanced treatment paradigms.

Acknowledgments

The authors acknowledge funding support from a University of Sydney International Research Collaboration Award. SL acknowledges support from project FP7-MSCA-PEOPLE-ITN-ARGENT (N°606381) and the Initiative de Recherche Strategique IRS Paris Saclay University NanoTheRad. The authors also wish to thank Yaser Gholami, Hilary Byrne, Erika Porcel and Jim Hainfeld for providing unpublished figures for this review article.

Conflicts of interest

None.

ORCID iDs

Zdenka Kuncic https://orcid.org/0000-0001-6765-3215

References

Adam J-F *et al* 2003 Synchrotron radiation therapy of malignant brain glioma loaded with an iodinated contrast agent: first trials on rats bearing F98 gliomas *Int. J. Radiat. Oncol. Biol. Phys.* **57** 1413

Al Zaki A *et al* 2014 Gold-loaded polymeric micelles for computed-tomography guided radiation therapy treatment and radiosensitization *ACS Nano* **8** 104

Antosh M P *et al* 2015 Enhancement of radiation effect on cancer cells by gold-pHLIP *Proc. Natl Acad. Sci.* **112** 5372

Asharani P V, Xinyi N, Hande M P and Valiyaveettil S 2010 DNA damage and p53-mediated growth arrest in human cells treated with platinum nanoparticles *Nanomedicine* **5** 51

Berbeco R I, Ngwa W and Makrigiorgos G M 2011 Localized dose enhancement to tumour blood vessel endothelial cells via megavoltage x-rays and targeted gold nanoparticles: new potential for external beam radiotherapy *Int. J. Radiat. Oncol. Biol. Phys.* **81** 270

Bhattarai S R *et al* 2017 Gold nanotriangles: scale up and x-ray radiosensitization effects in mice *Nanoscale* **9** 5085

Boudaiffa B, Cloutier P, Hunting D, Huels M A and Sanche L 2000 Resonant formation of DNA strand breaks by low-energy (3 to 20 eV) electrons *Science* **287** 1658

Bridot J-L *et al* 2007 Hybrid gadolinium oxide nanoparticles: multimodal contrast agents for *in vivo* imaging *J. Am. Chem. Soc.* **129** 5076

Briggs A *et al* 2013 Cerium oxide nanoparticles: influence of the high-Z component revealed on radioresistant 9L cell survival under x-ray radiation *Nanomedicine* **9** 1098

Brivio D *et al* 2015 Kilovoltage radiosurgery with gold nanoparticles for neovascular age-related macular degeneration (AMD): a Monte Carlo evaluation *Phys. Med. Biol.* **60** 9203

Butterworth K T, McMahon S J, Currell F J and Prise K M 2012 Physical basis and biological mechanisms of gold nanoparticle radiosensitization *Nanoscale* **4** 4830

Butterworth K T, McMahon S J, Taggart L E and Prise K M 2013 Radiosensitization by gold nanoparticles: effective at megavoltage energies and potential role of oxidative stress *Transl. Cancer Res.* **2** 269

Byrne H L, McNamara A L, Domanova W, Guatelli S and Kuncic Z 2013 Radiation damage on subcellular scales: beyond DNA *Phys. Med. Biol.* **58** 1251

Byrne H L, Gholami Y and Kuncic Z 2017 Impact of fluorescence from gold atoms on surrounding biological tissue—implications for nanoparticle radio-enhancement *Phys. Med. Biol.* **62** 3097

Carter J D, Cheng N N, Qu Y, Suarez G D and Guo T 2007 Nanoscale energy deposition by x-ray absorbing nanostructures *J. Phys. Chem.* B **111** 11622

Chetty I J *et al* 2015 Technology for innovation in radiation oncology *Int. J. Radiat. Oncol. Biol. Phys.* **93** 485

Chithrani D B *et al* 2010 Gold nanoparticles as radiation sensitizers in cancer therapy *Radiat. Res.* **173** 719

Cho S H 2005 Estimation of tumour dose enhancement due to gold nanoparticles during typical radiation treatments: a preliminary Monte Carlo study *Phys. Med. Biol.* **50** N163

Cho S H, Jones B L and Krishnan S 2009 The dosimetric feasibility of gold nanoparticle-aided radiation therapy (GNRT) via brachytherapy using low-energy gamma-/x-ray sources *Phys. Med. Biol.* **54** 4889

Cho J, Gonzalez-Lepera C, Manohar N, Kerr M, Krishnan S and Cho S H 2016 Quantitative investigation of physical factors contributing to gold nanoparticle-mediated proton dose enhancement *Phys. Med. Biol.* **61** 2562

Choi G-H *et al* 2012 Photon activated therapy (PAT) using monochromatic synchrotron x-rays and iron oxide nanoparticles in a mouse tumor model: feasibility study of PAT for the treatment of superficial malignancy *Radiat. Oncol.* **7** 184

Cooper D R, Bekah D and Nadeau J L 2014 Gold nanoparticles and their alternatives for radiation therapy enhancement *Front. Chem.* **2** 86
Corde S *et al* 2002 Lack of cell death enhancement after irradiation by monochromatic synchrotron x-rays at the *K*-shell edge of platinum incorporated in living SQ20B human cells as cis-diamminedichloroplatinum (II) *Radiat. Res.* **158** 763
Danhier F 2016 To exploit the tumor microenvironment: since the EPR effect fails in the clinic, what is the future of nanomedicine? *J. Control. Rel.* **244** 108
Davis M E, Chen Z and Shin D M 2008 Nanoparticle therapeutics: an emerging treatment modality for cancer *Nat. Rev. Drug Discovery* **7** 771
De Barros A L B, Tsourkas A, Saboury B, Cardoso V N and Alavi A 2012 Emerging role of radiolabeled nanoparticles as an effective diagnostic technique *Eur. J. Nucl. Med. Mol. Imaging Res.* **2** 39
Detappe A, *et al* 2015 AGuIX nanoparticles as a promising platform for image-guided radiation therapy *Cancer Nano* **6** 4
Detappe A *et al* 2016 Advanced multimodal nanoparticles delay tumor progression with clinical radiation therapy *J. Control. Rel.* **238** 103
Detappe A *et al* 2017 Ultrasmall silica-based bismuth gadolinium nanoparticles for dual magnetic resonance imaging-computed tomography image guided radiation therapy *Nano Lett.* **17** 1733
Dou Y *et al* 2016 Size-tuning ionization to optimize gold nanoparticles for simultaneous enhanced CT imaging and radiotherapy *ACS Nano* **10** 2536
Douglass M, Bezak E and Penfold S 2013 Monte Carlo investigation of the increased radiation deposition due to gold nanoparticles using kilovoltage and megavoltage photons in a 3D randomized cell model *Med. Phys.* **40** 071710
Dufort S *et al* 2016 The high radiosensitizing efficiency of a trace of gadolinium-based nanoparticles in tumors *Sci. Rep.* **6** 29678
Durante M, Orecchia R and Loeffler J S 2017 Charged-particle therapy in cancer: clinical uses and future perspectives *Nat. Rev. Clin. Oncol.* **14** 483
Edouard M, Broggio D, Prezado Y, Esteve F, Elleaume H and Adam J F 2010 Treatment plans optimization for contrast-enhanced synchrotron stereotactic radiotherapy *Med. Phys.* **37** 2445
Evans R D 1955 *The Atomic Nucleus* (New York: McGraw-Hill)
Fano U 1963 Penetration of protons, alpha particles and mesons *Ann. Rev. Nuc. Sci.* **13** 1
Fano U 1992 A common mechanism of collective phenomena *Rev. Mod. Phys.* **64** 313
Favaudon V *et al* 2014 Ultrahigh dose-rate FLASH irradiation increases the differential response between normal and tumor tissue in mice *Sci. Transl. Med.* **6** 245ra93
Fouillade C *et al* 2017 Hopes of high dose-rate radiotherapy *Bull. Cancer* **104** 380
Gao Y, Chen K, Ma J L and Gao F 2014 Cerium oxide nanoparticles in cancer *Onco Targets Ther.* **7** 835
Garnica-Garza H M 2011 Treatment planning considerations in contrast-enhanced radiotherapy: energy and beam aperture optimization *Phys. Med. Biol.* **56** 341
Gehrke H *et al* 2011 Platinum nanoparticles and their cellular uptake and DNA platination at non-cytotoxic concentrations *Arch. Toxicol.* **85** 799
Gokhberg K, Kolorenc P, Kuleff A L and Cederbaum L S 2014 Site- and energy-selective slow-electron production through intermolecular Coulombic decay *Nat.* **505** 661
Grall R *et al* 2015 Impairing the radioresistance of cancer cells by hydrogenated nanodiamonds *Biomaterials* **61** 290
Hainfeld J F, Slatkin D N and Smilowitz H N 2004 The use of gold nanoparticles to enhance radiotherapy in mice *Phys. Med. Biol.* **49** N309
Hainfeld J F, Dilmanian F A, Slatkin D N and Smilowitz H M 2008 Radiotherapy enhancement with gold nanoparticles *J. Pharm. Pharmacol.* **60** 977
Hainfeld J F, Smilowitz H M, O'Connor M J, Dilmanian F A and Slatkin D N 2013 Gold nanoparticle imaging and radiotherapy of brain tumors in mice *Nanomedicine* **8** 1601
Hainfeld J F, Lin L, Slatkin D N, Dilmanian F A, Vadas T M and Smilowitz H M 2014 Gold nanoparticle hyperthermia reduces radiotherapy dose *Nanomedicine* **10** 1609
Hatano Y, Katsumura Y and Mozumder A (ed) 2010 *Charged Particle and Photon Interactions with Matter: Recent Advances, Applications and Interfaces* (Boca Raton, FL: CRC Press)
Herold D M, Das I J, Stobbe C C, Iyer R V and Chapman J D 2000 Gold microspheres: A selective technique for producing biologically effective dose enhancement *Int. J. Radiat. Biol.* **76** 1357
Haume K *et al* 2016 Gold nanoparticles for cancer radiotherapy: a review *Cancer Nanotechnol.* **7** 8
Huang F-K *et al* 2010 Enhancement of irradiation effects on cancer cells by cross-linked dextran-coated iron oxide (CLIO) nanoparticles *Phys. Med. Biol.* **55** 469
Jahnke T *et al* 2010 Ultrafast energy transfer between water molecules *Nat. Phys.* **6** 139
Jain S, Hirst D G and O'Sullivan J M 2012 Gold nanoparticles as novel agents for cancer therapy *Br. J. Radiol.* **85** 101
Jeynes J C G, Merchant M J, Spindler A, Wera A C and Kirkby K J 2014 Investigation of gold nanoparticle radiosensitization mechanisms using a free radical scavenger and protons of different energies *Phys. Med. Biol.* **59** 6431
Jiang W, Kim B Y S, Rutka J T and Chan W C W 2008 Nanoparticle-mediated celular response is size-dependent *Nat. Nanotechnol.* **3** 145
Kam W W-Y *et al* 2013 Predicted ionization in mitochondria and acute changes in the mitochondrial transcriptome after gamma irradiation: a Monte Carlo and quantitative PCR study *Mitochondrion* **13** 736
Kaur H, Pujari G, Semwal M K, Sarma A and Avasthi D K 2013 *In vitro* studies on radiosensitization effect of glucose capped gold nanoparticles in photon and ion irradiation of HeLa cells *Nucl. Inst. Meth. Phys. Res.* B **301** 7
Khoei S, Mahdavi S R, Fakhimikabir H, Shakeri-Zadeh A and Hashemian A 2014 The role of iron oxide nanoparticles in the radiosensitization of human prostate carcinoma cell line DU145 at megavoltage radiation energies *Int. J. Rad. Biol.* **90** 351
Kim J-K, *et al* 2010 Therapeutic application of metallic nanoparticles combined with particle-induced x-ray emission effect *Nanotechnology* **21** 425102
Kim J-K *et al* 2012 Enhanced proton treatment in mouse tumors through proton irradiated nanoradiator effects on metallic nanoparticles *Phys. Med. Biol.* **57** 8309
Kittel C 1963 *Quantum Theory of Solids* 2nd edn (New York: Wiley)
Klein S *et al* 2014 Superparamagnetic iron oxide nanoparticles as novel x-ray enhancer for low-dose radiation therapy *J. Phys. Chem.* B **118** 6159
Kobayashi K, Frohlich H, Usami N, Takahura K and Le Sech C 2002 Enhancement of x-ray induced breaks in DNA bound to molecules containing platinum: a possible application to hadrontherapy *Radiat. Res.* **157** 32
Kobayashi K, Usami N, Porcel E, Lacombe S and Le Sech C 2010 Enhancement of radiation effect by heavy elements *Mutat. Res.* **704** 123
Kong T *et al* 2008 Enhancement of radiation cytotoxicity in breast cancer cells by localized attachment of gold nanoparticles *Small* **4** 1537
Kotb S *et al* 2016 Gadolinium-based nanoparticles and radiation therapy for multiple brain melanoma metastases: proof of concept before phase I trial *Theranostics* **6** 418

Kuncic Z 2015 Advances in computational radiation biophysics for cancer therapy: simulating nano-scale damage by low-energy electrons *Biophys. Rev. Lett.* **10** 40
Kuncic Z *et al* 2012 *In silico* nanodosimetry: new insights into radiation-induced biological damage *Comput. Math. Meth. Med.* **2012** 147252
Kunjachan S *et al* 2015 Nanoparticle mediated tumor vascular disruption: a novel strategy in radiation therapy *Nano Lett.* **15** 7488
Lacombe S, Porcel E and Scifoni E 2017 Particle therapy and nanomedicine: state of the art and research perspective *Cancer Nanotechnol.* **8** 9
Lammers T *et al* 2008 Image-guided and passively tumour-targeted polymeric nanomedicines for radiochemotherapy *Br. J. Cancer* **99** 900
Laurent G *et al* 2016 Minor changes in the macrocyclic ligands but major consequences on the efficiency of gold nanoparticles designed for radiosensitization *Nanoscale* **8** 12054
Le Duc G *et al* 2011 Toward an image-guided microbeam radiation therapy using gadolinium-based nanoparticles *ACS Nano* **5** 9566
Lechtman E *et al* 2011 Implications on clinical scenario of gold nanoparticle radiosensitisation in regards to photon energy, nanoparticle size, concentration and location *Phys. Med. Biol.* **56** 4631
Lechtman E *et al* 2013 A Monte Carlo-based model of gold nanoparticle radiosensitization accounting for increased radiobiological effectiveness *Phys. Med. Biol.* **58** 3075
Lee D S, Im H-J and Lee Y-S 2015 Radionanomedicine: widened perspectives of molecular theragnostics *Nanomedicine* **11** 795
Leung M K K *et al* 2011 Irradiation of gold nanoparticles by x-rays: Monte Carlo simulation of dose enhancements and the spatial properties of the secondary electrons production *Med. Phys.* **38** 624
Li T *et al* 2016 Thermosensitive hydrogel co-loaded with gold nanoparticles and doxorubicin for effective chemoradiotherapy *Am. Assoc. Pharm. Sci. J.* **18** 146
Lin Y, McMahon S J, Scarpelli M, Paganetti H and Schuemann J 2014 Comparing gold nano-particle enhanced radiotherapy with protons, megavoltage photons and kilovoltage photons: a Monte Carlo simulation *Phys. Med. Biol.* **59** 7675
Lin Y, McMahon S J, Paganetti H and Schuemann J 2015 Biological modeling of gold nanoparticle enhanced radiotherapy for proton therapy *Phys. Med. Biol.* **60** 4149
Liu Y *et al* 2015 The dependence of radiation enhancement effect on the concentration of gold nanoparticles exposed to low- and high-LET radiations *Phys. Med.* **31** 210
Liu Y *et al* 2016 The radiation enhancement of 15 nm citrate-capped gold nanoparticles exposed to 70 keV μm^{-1} carbon ions *J. Nanosci. Nanotechnol.* **16** 3
Luchette M, Korideck H, Makrigiorgos M, Tillement O and Berbeco R 2014 Radiation dose enhancement of gadolinium-based AGuIX nanoparticles on HeLa cells *Nanomedicine* **10** 1751
Lux F *et al* 2015 Gadolinium-based nanoparticles for theranostic MRI-radiosensitization *Nanomedicine* **10** 1801
Maggiorella L *et al* 2012 Nanoscale radiotherapy with hafnium oxide nanoparticles *Future Oncol.* **8** 1167
Manohar N *et al* 2016 Quantitative imaging of gold nanoparticle distribution in a tumor-bearing mouse using benchtop x-ray fluorescence computed tomography *Sci. Rep.* **6** 22079
Martinez-Rovira I and Prezado Y 2015 Evaluation of the local dose enhancement in the combination of proton therapy and nanoparticles *Med. Phys.* **42** 6703
McKinnon S *et al* 2016 Local dose enhancement of proton therapy by ceramic oxide nanoparticles investigated with Geant4 simulations *Phys. Med.* **32** 1584
McMahon S J *et al* 2011a Biological consequences of nanoscale energy deposition near irradiated heavy atom nanoparticles *Sci. Rep.* **1** 18
McMahon S J *et al* 2011b Nanodosimetric effects of gold nanoparticles in megavoltage radiation therapy *Radiother. Oncol.* **100** 412
McMahon S J *et al* 2011c Energy dependence of gold nanoparticle radiosensitization in plasmid DNA *J. Phys. Chem.* C **115** 20160
McMahon S J, Paganetti H and Prise K M 2016 Optimising element choice for nanoparticle radiosensitisers *Nanoscale* **8** 581
McMahon S J, McNamara A L, Schuemann J, Prise K M and Paganetti H 2017 Mitochondria as a target for radiosensitisation by gold nanoparticles *J. Phys.: Conf. Ser.* **777** 012008
McNamara A L *et al* 2016 Dose enhancement effects to the nucleus and mitochondria from gold nanoparticles in the cytosol *Phys. Med. Biol.* **61** 5993
McQuade C *et al* 2015 A multifunctional nanoplatform for imaging, radiotherapy and the prediction of therapeutic response *Small* **11** 834
McQuade C *et al* 2016 Imaging and radiation effects of gold nanoparticles in tumour cells *Sci. Rep.* **6** 19442
Mignot A *et al* 2013 A top-down synthesis route to ultrasmall multifunctional Gd-based silica nanoparticles for theranostic applications *Chem. Eur. J.* **19** 6122
Miladi I *et al* 2014 The *in vivo* radiosensitizing effect of gold nanoparticles based MRI contrast agents *Small* **10** 1116
Montay-Gruel P *et al* 2017 Irradiation in a flash: unique sparing of spatial memory in mice after whole brain irradiation with dose rates above 100 Gy/s *Radiother. Oncol.* **124** 365
Mucke M *et al* 2010 A hitherto unrecognized source of low-energy electrons in water *Nat. Phys.* **6** 143
Mura S and Couvreur P 2012 Nanotheranostics for personalized medicine *Adv. Drug Deliv. Rev.* **64** 1394
Normandin M D *et al* 2015 Heat-induced radiolabeling of nanoparticles for monocyte tracking by PET *Angew. Chem., Int. Ed.* **54** 13002
Pan X, Cloutier P, Hunting D and Sanche L 2003 Dissociative electron attachment to DNA *Phys. Rev. Lett.* **90** 208102
Perl J, Shin J, Schuemann J, Faddegon B and Paganetti H 2012 TOPAS: an innovative proton Monte Carlo platform for research and clinical applications *Med. Phys.* **39** 6818
Perrault S D, Walkey C, Jennings T, Fischer H C and Chan W C 2009 Mediating tumor targeting efficiency of nanoparticles through design *Nano Lett.* **9** 1909
Polf J C, *et al* 2011 Enhanced relative biological effectiveness of proton radiotherapy in tumor cells with internalized gold nanoparticles *Appl. Phys. Lett.* **98** 193702
Popovtzer A *et al* 2016 Actively targeted gold nanoparticles as novel radiosensitizer agents: an *in vivo* head and neck cancer model *Nanoscale* **5** 2678
Porcel E *et al* 2010 Platinum nanoparticles: a promising material for future cancer therapy? *Nanotechnology* **21** 085103
Porcel E, *et al* 2012 Nano-sensitization under gamma rays and fast ion irradiation *J. Phys.: Conf. Ser.* **373** 012006
Porcel E *et al* 2014 Gadolinium-based nanoparticles to improve the hadrontherapy performances *Nanomedicine* **10** 1601
Robar J L, Riccio S A and Martin M A 2002 Tumour dose enhancement using modified megavoltage photon beams and contrast media *Phys. Med. Biol.* **47** 5487
Sancey L *et al* 2014 The use of theranostic gadolinium-based nanoprobes to improve radiotherapy efficacy *Br. J. Radiol.* **87** 20140314
Schlatholter T *et al* 2016 Improving proton therapy by metal-containing nanoparticles: nanoscale insights *Int. J. Nanomed.* **11** 1549
Schuemann J *et al* 2016 Roadmap to clinical use of gold nanoparticles for radiosensitization *Int. J. Radiat. Oncol. Biol. Phys.* **94** 189
Seiwert T Y, Salama J K and Vokes E E 2007 The concurrent chemoradiation paradigm—general principles *Nat. Clin. Pract. Oncol.* **4** 86
Stefancikova L *et al* 2014 Cell localization of gadolinium-based nanoparticles and related radiosensitising efficacy in glioblastoma cells *Cancer Nano* **5** 6

Stumpf V, Gokhberg K and Cederbaum L S 2016 The role of metal ions in x-ray-induced photochemistry *Nat. Chem.* **8** 237
Stumpf V, Kolorenc P, Gokhberg K and Cederbaum L S 2013 Efficient pathway to neutralization of multiply charged ions produced in Auger processes *Phys. Rev. Lett.* **110** 258302
Su N, Dang Y, Liang G and Liu G 2015 Iodine-125 labeled cRGD-gold nanoparticles as tumor-targeted radiosensitizer and imaging agent *Nanoscale Res. Lett.* **10** 160
Taggart L E, McMahon S J, Currell F J, Prise K M and Butterworth K T 2014 The role of mitochondrial function in gold nanoparticle mediated radiosensitisation *Cancer Nano* **5** 5
Taupin F *et al* 2015 Gadolinium nanoparticles and contrast agent as radiation sensitizers *Phys. Med. Biol.* **60** 4449
Thorek D L J *et al* 2014 Non-invasive mapping of deep-tissue lymph nodes in live animals using a multimodal PET/MRI nanoparticle *Nat. Commun.* **5** 3097
Toy R, Peiris P, Ghaghada K B and Karathanasis E 2014 Shaping cancer nanomedicine: the effect of particle shape on the *in vivo* journey of nanoparticles *Nanomedicine* **9** 121
Twyman-Saint Victor C *et al* 2015 Radiation and dual checkpoint blockade activate non-redundant immune mechanisms in cancer *Nature* **520** 373
Usami N *et al* 2008 Mammalian cells loaded with platinum-containing molecules are sensitized to fast atomic ions *Int. J. Radiat. Biol.* **84** 603
Verkhovtsev A V, Korol A V and Solov'yov A V 2015a Revealing the mechanism of the low-energy electron yield enhancement from sensitizing nanoparticles *Phys. Rev. Lett.* **114** 063401
Verkhovtsev A V, Korol A V and Solov'yov A V 2015b Electron production by sensitizing gold nanoparticles irradiated by fast ions *J. Phys. Chem.* C **119** 11000
Verkhovtsev A V, Korol A V and Solov'yov A V 2016a Irradiation-induced processes with atomic clusters and nanoparticles *Nanoscale Insights Into Ion-Beam Cancer Therapy* ed A V Solov'yov (Cham: Springer) p 237
Verkhovtsev A V, Surdutovich E and Solov'yov A V 2016b Multiscale approach predictions for biological outcomes in ion-beam cancer therapy *Sci. Rep.* **6** 27654
Wälzlein C, Scifoni E, Kramer M and Durante M 2014 Simulations of dose enhancement for heavy atom nanoparticles irradiated by protons *Phys. Med. Biol.* **59** 1441
Wolfe T *et al* 2015 Targeted gold nanoparticles enhance sensitization of prostate tumors to megavoltage radiation therapy *in vivo* *Nanomedicine* **11** 1277
Xiao F *et al* 2011 On the role of low energy electrons in the radiosensitization of DNA by gold nanoparticles *Nanotechnology* **22** 465101
Yang L X, Douple E B, O'Hara J A and Wang H J 1995 Production of double strand breaks by interactions between carboplatin and radiation: a potential mechanism for radioprotection *Radiat. Res.* **143** 309
Yang Y-S, Carney R P, Stellaci F and Irvine D J 2014 Enhancing radiotherapy by lipid nanocapsule-mediated delivery of amphiphilic gold nanoparticles to intracellular membranes *ACS Nano* **8** 8992
Yook S *et al* 2015 Radiation nanomedicine for EGFR-positive breast cancer: Panitumumab-modified gold nanoparticles complexed to the β-particle emitter ^{177}Lu *ACS Mol. Pharmaceut.* **12** 3963
Zhang X *et al* 2008 Enhanced radiation sensitivity in prostate cancer by gold nanoparticles *Clin. Invest. Med.* **31** E160
Zhang L *et al* 2010 Delivery of therapeutic radioisotopes using nanoparticle platforms: potential benefit in systemic radiation therapy *Nanotechnol. Sci. Appl.* **3** 159
Zhang X-D *et al* 2015 Ultrasmall glutathione-protected hold nanoclusters as next generation radiotherapy sensitizers with high tumor uptake and high renal clearance *Sci. Rep.* **5** 8669
Zygmanski P, Liu B, Tsiamas P, Cifter F, Petersheim M, Hesser J and Sajo E 2013 Dependence of Monte Carlo microdosimetric computations on the simulation geometry of gold nanoparticles *Phys. Med. Biol.* **58** 7961